TIME RESOLVED CARS

FREQUENCY DOMAIN

UNIVERSITY OF ARIZONA
DEPARTMENT OF CHEMISTRY
85 721 TUSCON, AZ, USA

- H. Abramczyk, Femtosecond primary events in bacteriorhodopsin. Revision of commonly accepted interpretation of electronic spectra of transient intermediates, J. Chem. Phys. 120 11120 (2004)
-
- A. Terentis, L. Uji, H. Abramczyk, G. H. Atkinson, Primary events in Bacteriorhodopsin photocycle: torsional vibrational dephasing in the first excited electronic state, Chem. Phys. 313(2005) 51-62

PICOSECOND CARS

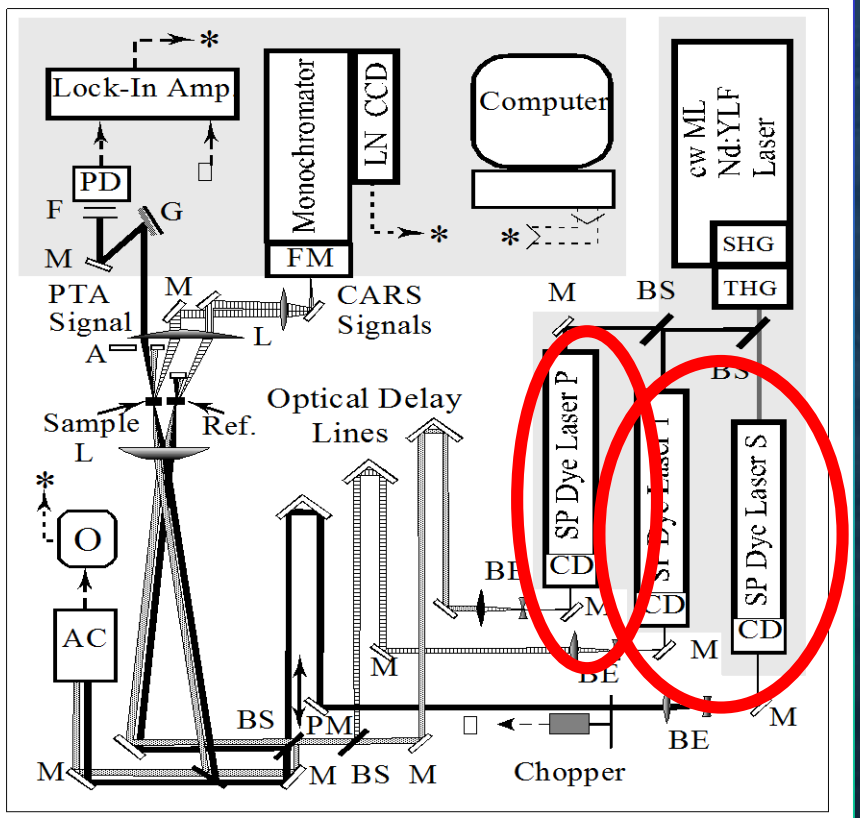

PUMP

PROBE

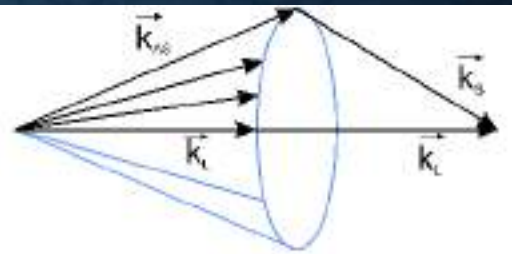

Fig. 4.5. Directions of propagation of the stimulated anti-Stokes scattering

Why the phase matching condition, $\Delta k = 0$, that is always met for the stimulated Stokes scattering, it is not automatically complied with the stimulated anti-Stokes scattering? It results from the fact that the phase of vibrating molecules is defined by the more intense Stokes scattering.

To sum up, intense light of the frequency ω_L can cause intense stimulated Raman scattering: Stokes $\omega_S = \omega_L - \omega_{vib}$ and anti-Stokes $\omega_{AS} = \omega_L + \omega_{vib}$. As a result of photon interaction with matter, the energy exchange via optical phonons (or vibrations) takes place leading to the formation in a medium the third-order polarisation, $P^{(3)} \propto \chi^{(3)}_{ijkl} E_j E_k E_l$, that consists of the components changing with the frequency $\omega_{vib} = \omega_L - \omega_S$, $\omega_S = \omega_L - \omega_{vib}$ and $\omega_{AS} = \omega_L + \omega_{vib}$. The polarisation components generate new waves of the frequencies ω_S and ω_{AS} known as the stimulated Stokes and anti-Stokes Raman scattering. The phase matching condition is met in all directions for the Stokes radiation ($\Delta k = 0$), so the scattered light is emitted in all directions. The anti-Stokes stimulated scattering is observed in directions, $\mathbf{k}_{AS}$, for which the phase matching condition $2\mathbf{k}_L - \mathbf{k}_S = \mathbf{k}_{AS}$ is met.

Briefly, lightpulses from a narrowband (<4 cm1, FWHM) dye laser operated at 663 nm (l1) and a broadband (700 cm1)dye laser operated in the 700–750 nm region (ls) are phase-matched in a flowing BR (native or modified-retinal pigment) sample, generating CARS signals spanning an approximately 700 cm1 spectral region (λas). In order to cover the entire 750–1750 cm1spectral range of interest, either λ1is tuned a few nanometers or λ s is adjusted by using a different laser-dye solution.

CARS: theory

- Intensity of the CARS signal:

$$I_{as}(\omega_{as}) \mu |\chi^{(3)}(\omega_{as}, \omega_1, \omega_s)|^2 . I_1^2 . I_s(\omega_s) . G^2$$

- Normalized CARS spectrum fitting function (2-species mixture):

$$\frac{I_{as}^{Sample}}{I_{as}^{Reference}} = \mu^2 \left| 1 + (1 - \eta) \sum_{j=1}^{N_A} \frac{A_j \, e^{i\Theta_j}}{\Delta_j - i} + \eta \sum_{k=1}^{N_B} \frac{A_k \, e^{i\Theta_k}}{\Delta_k - i} \right|^2$$

$$\Delta_j = (\Omega_j - (\omega_1 - \omega_s)) / \Gamma_j$$

- Background-free (Lorentzian lineshapes) spectral intensity:

$$I_{raman} = \sum_{j=1}^{N} \frac{A_j^2}{(\Omega_j - (\omega_1 - \omega_s))^2 + \Gamma_j^2}$$

Ω = Band Origin
A = Amplitude
Γ = Bandwidth
Θ = Vibrational phase
η = relative conc.(0£ η £1)
μ = Scaling factor
N = Number of vibrations
$\chi^{(3)}$ = third-order susceptibility

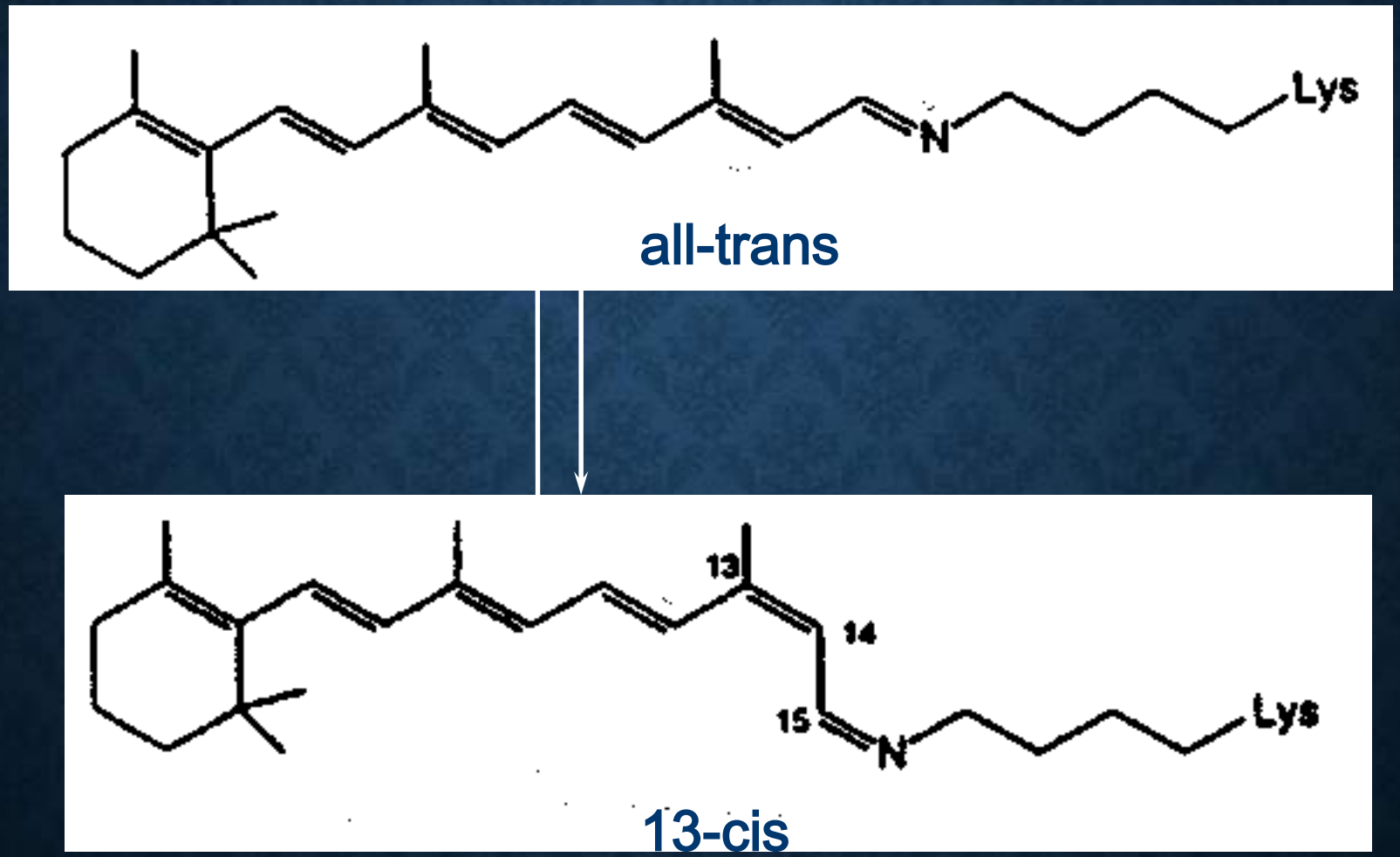

Light activation *triggers* trans to cis isomerization of a bound retinal

Native BR-568 and unlocked analogs BR 6.11 and 6.9

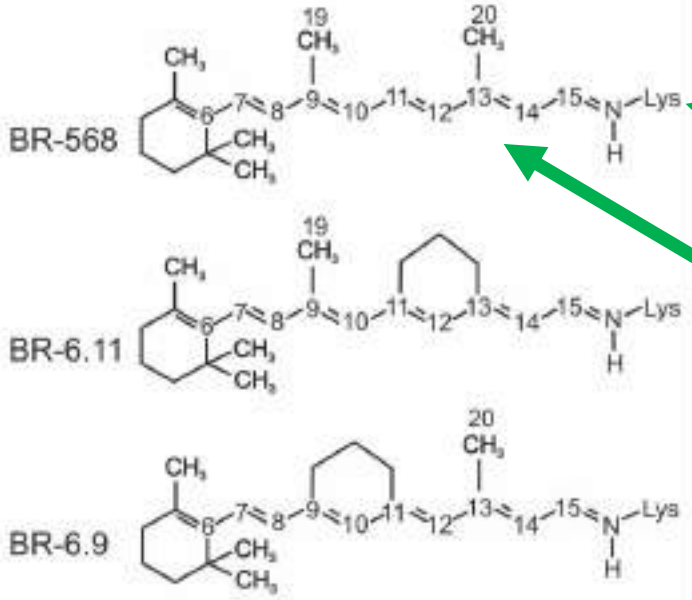

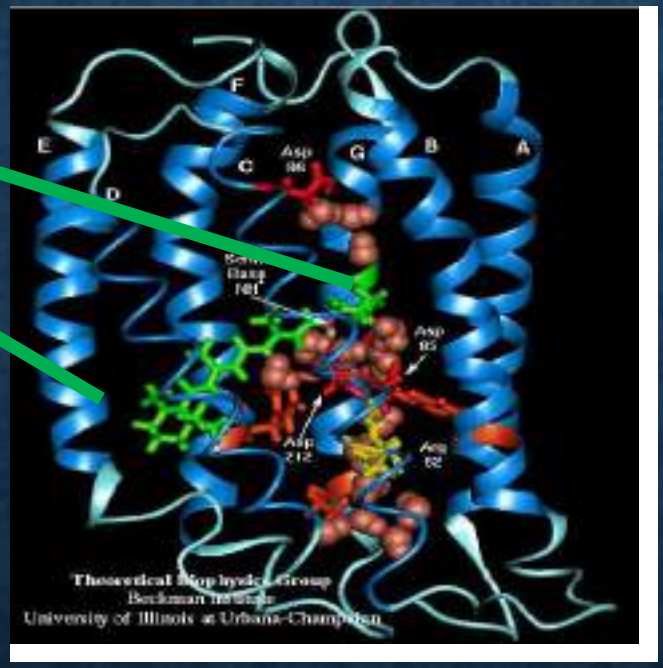

Locked analogs BR 5.12 and BR 5.13

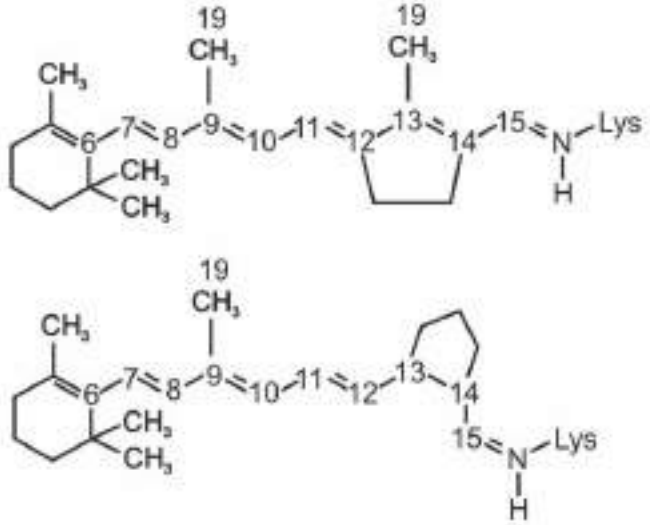

Andrew C. Terentis, Laszlo Ujj, Halina Abramczyk, George H. Atkinson*
Chemical Physics 313 (2005) 51–6

NATIVE BR-568 AND UNLOCKED ANALOGS BR 6.11 AND 6.9

The artificial BR pigments examined here contain a retinal with six-membered carbon ring incorporated into the retinal backbone that remains the 13C=C14 bond free to isomerize

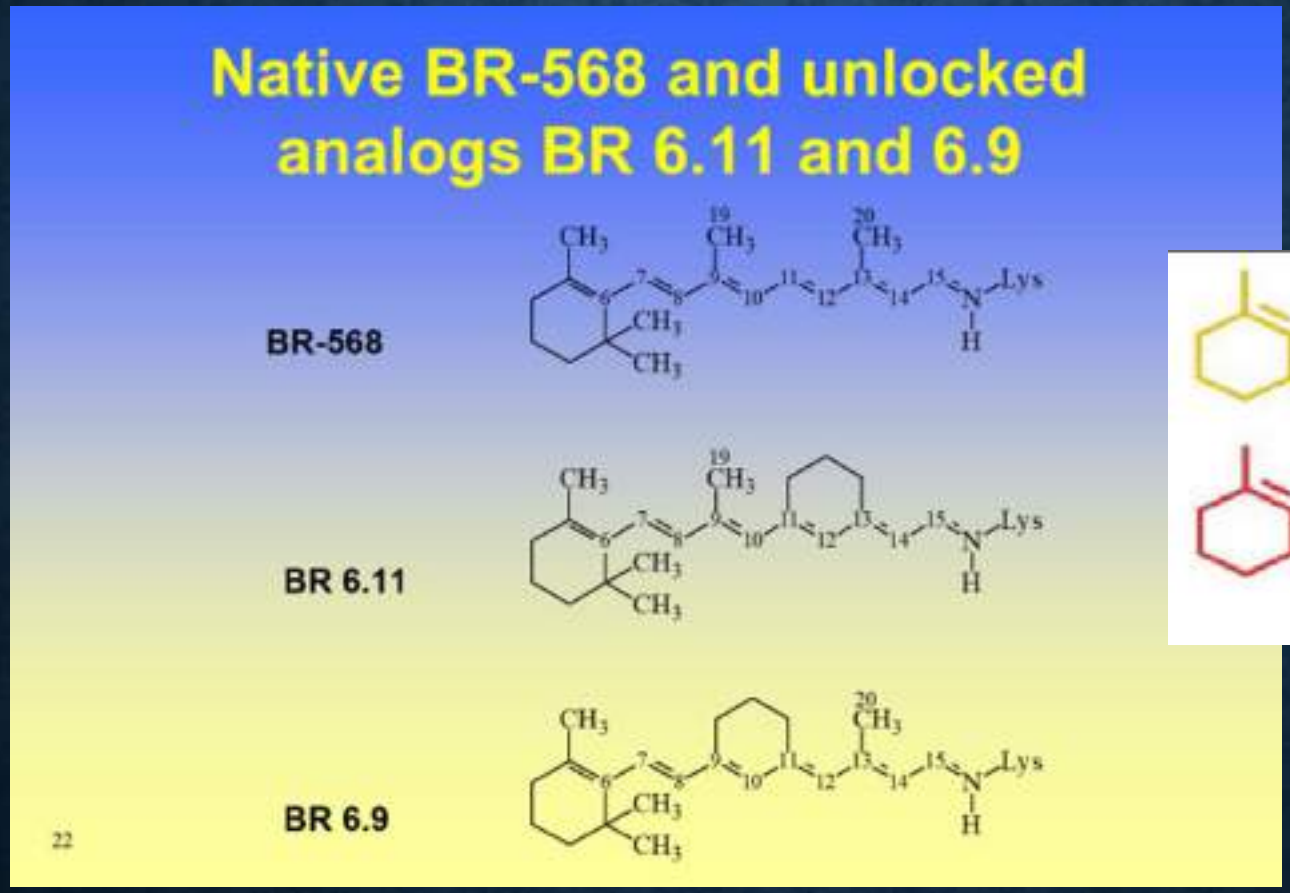

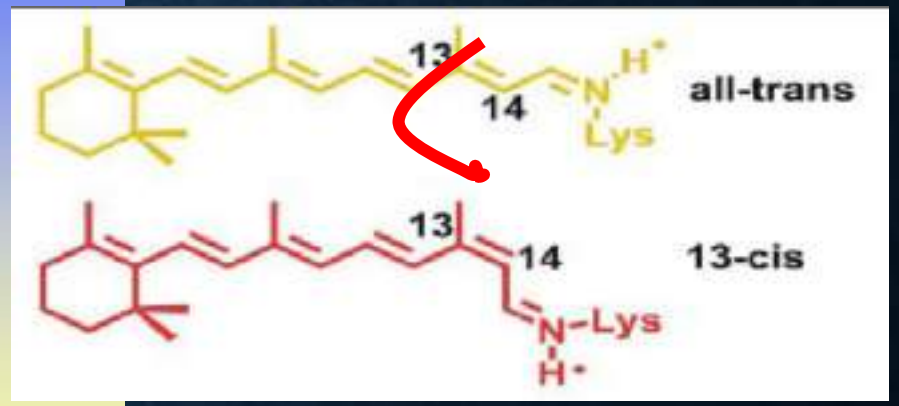

Primary events in the bacteriorhodopsin photocycle:Torsional vibrational dephasing in the first excited electronic stateAndrew C. Terentis, Laszlo Ujj, Halina Abramczyk, George H. Atkinson* Chemical Physics 313 (2005) 51–6

Locked analogs BR 5.12 and BR 5.13

BR 5.12

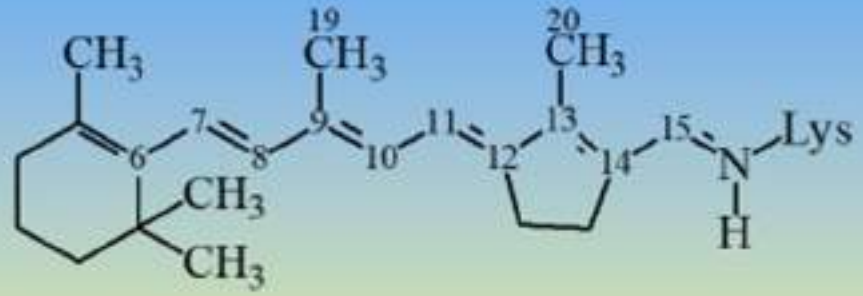

BR 5.13

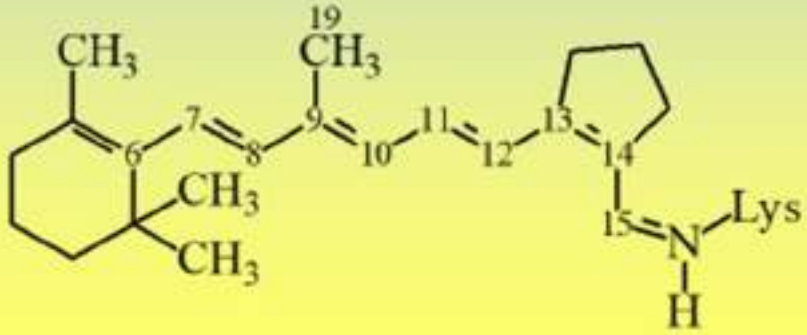

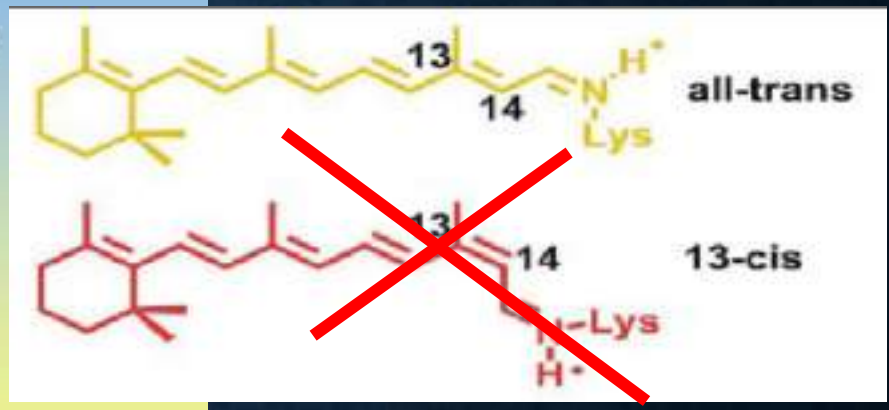

28

For BR5.12, the C13=C14 retinal bond is locked in the trans configuration by a rigid, five-membered carbon ring

NATIVE BR-568 AND UNLOCKED ANALOGS BR 6.11 AND 6.9

The artificial BR pigments examined here contain a retinal with six-membered carbon ring incorporated into the retinal backbone that remains the 13C=C14 bond free to isomerize

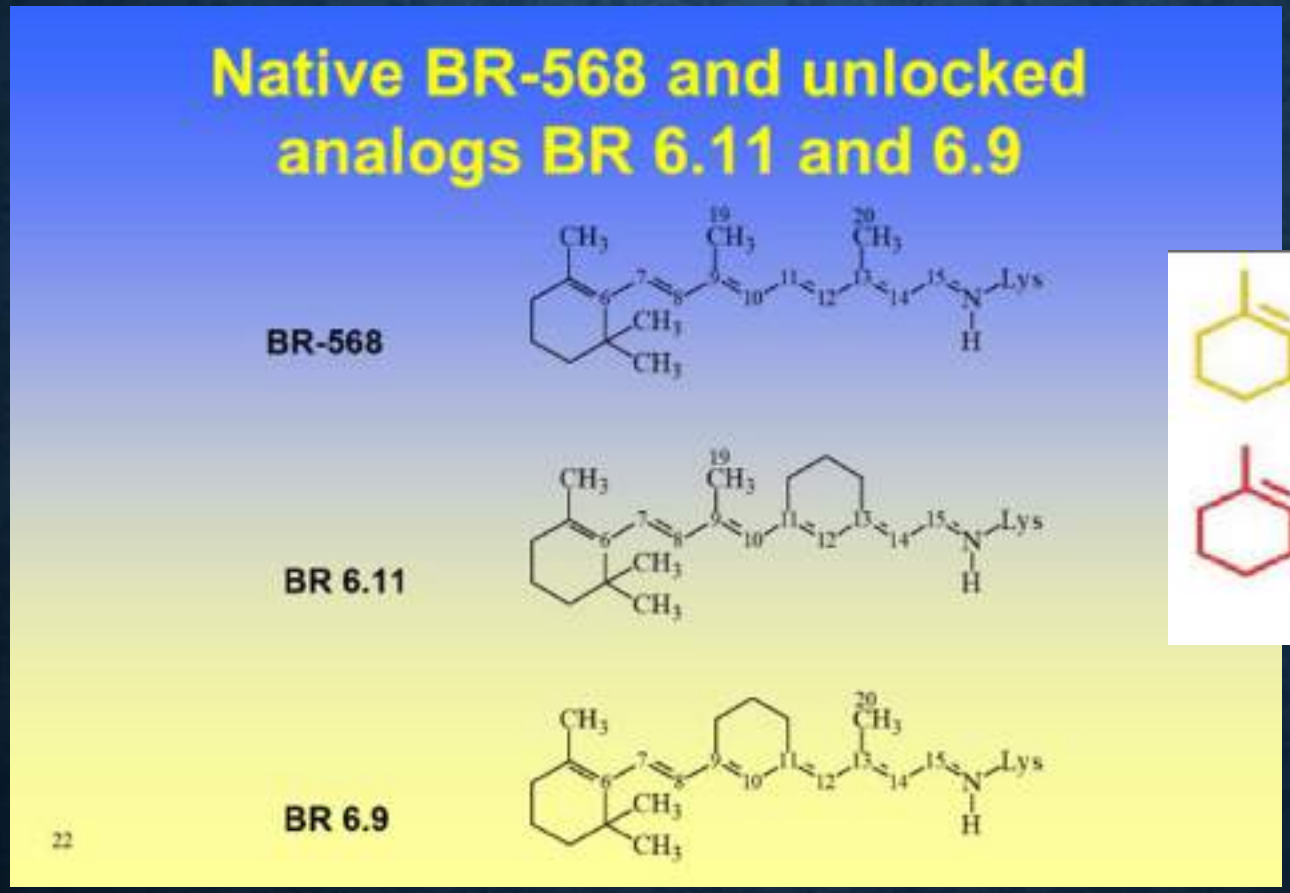

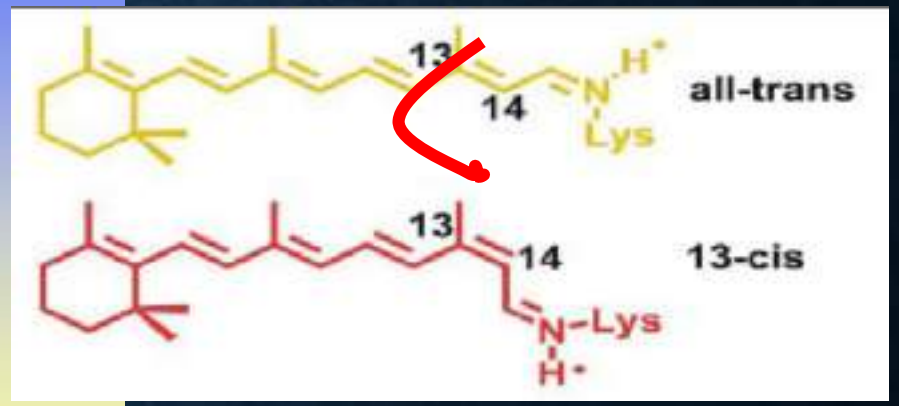

Primary events in the bacteriorhodopsin photocycle:Torsional vibrational dephasing in the first excited electronic stateAndrew C. Terentis, Laszlo Ujj, Halina Abramczyk, George H. Atkinson* Chemical Physics 313 (2005) 51–6

NATIVE BR-568 AND UNLOCKED ANALOGS BR 6.11 AND 6.9

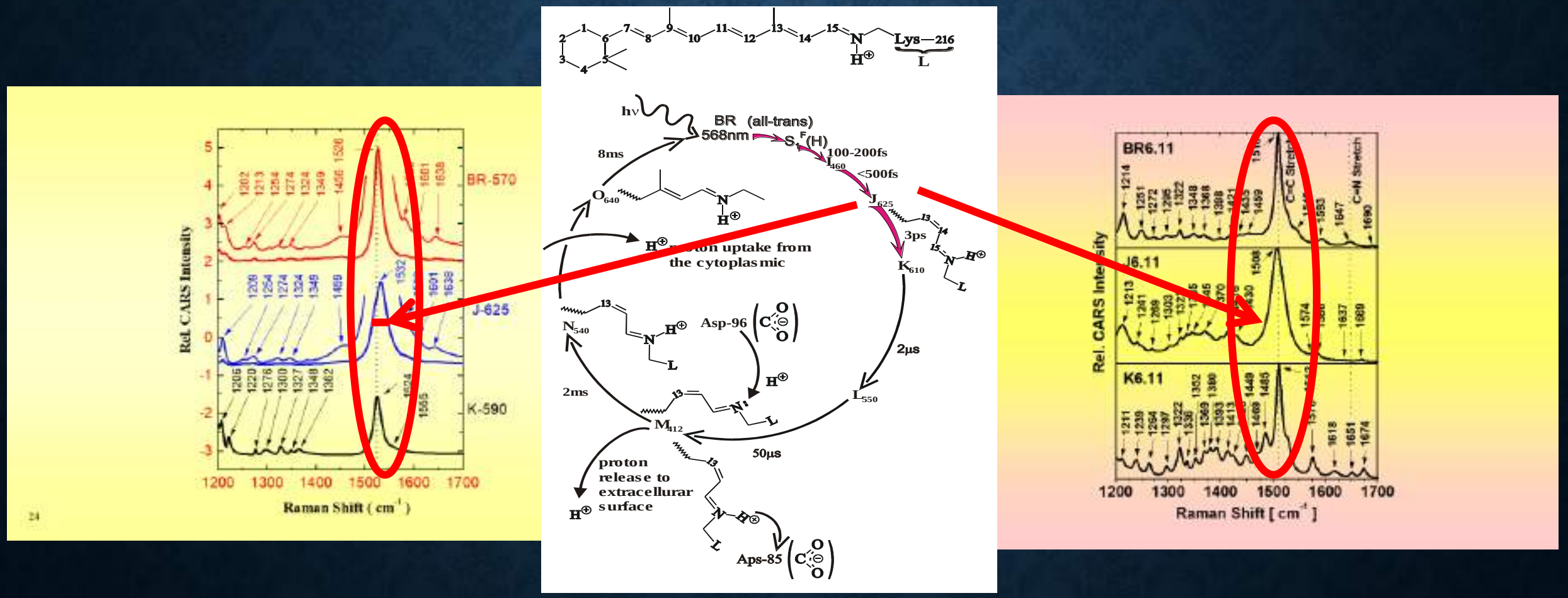

vibrational spectra of BR-570 (top), J-625 (center, derived from the 0-ps PTR/CARS data),and K-590 (bottom, derived from the 200-ps PTR/CARS data) in the1200–1700 cm1region

Locked analogs BR 5.12 and BR 5.13

BR 5.12

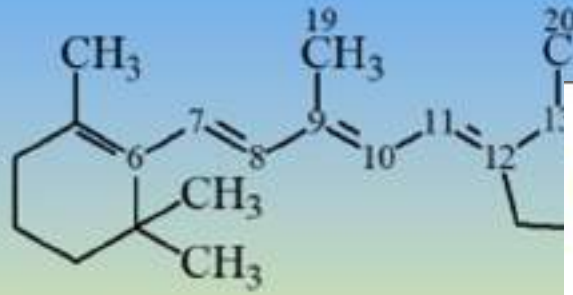

BR 5.13

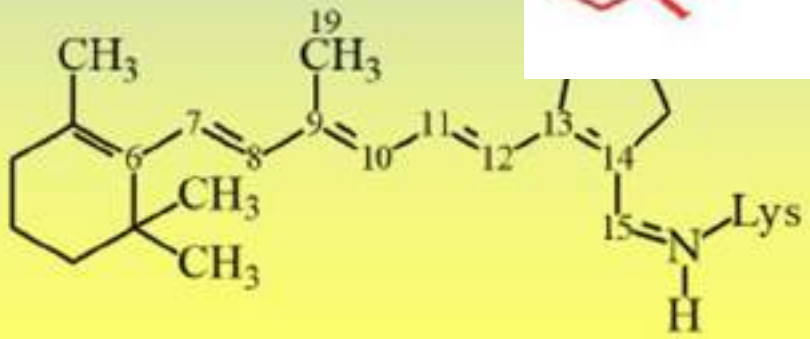

28

Andrew C. Terentis, Laszlo Ujj, Halina Abramczyk, George H. Atkinson* Chemical Physics 313 (2005) 51–6

For BR5.12, the C13=C14 retinal bond is locked in the trans configuration by a rigid, five-membered carbon ring

Locked analogs BR 5.12 and BR 5.13

BR 5.12

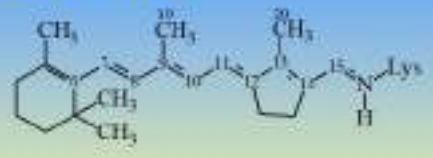

BR 5.13

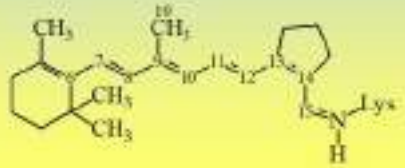

Andrew C. Terentis, Laszlo Ujj, Halina Abramczyk, George H. Atkinson*
Chemical Physics 313 (2005) 51–6

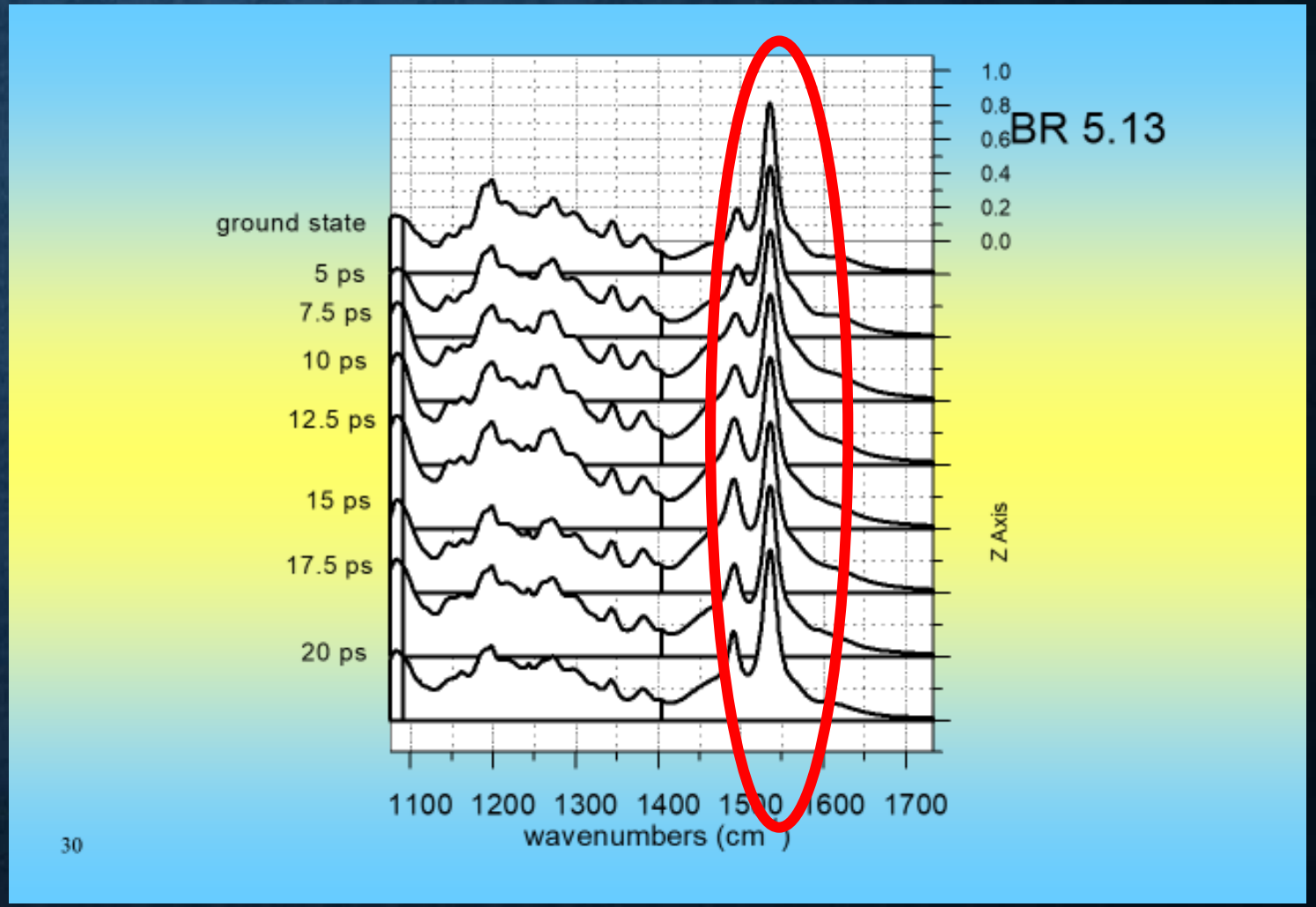

WHAT INFORMATION ABOUT VIBRATIONAL DYNAMICS IS CONTAINED IN THE CARS BAND SHAPE ?

1 Maxwell equation

$$\nabla^2 E + \frac{1}{c^2}\frac{\partial^2 (E(\vec{r},t))}{\partial t^2} = -\frac{4\pi}{c^2}\frac{\partial^2 P}{\partial t^2}$$

2 $\langle \vec{P}(\vec{r},t) \rangle = T_r\left(\vec{P}(\vec{r},t)\right)\rho(t)$ density operator

3

$$\frac{\partial \rho}{\partial t} = -\frac{i}{\hbar}[H(t),\rho] \rightarrow \rho(t) = \rho_0 \exp(-iHt)$$

$H(t) = H_0$

$$\rho = \rho^0 + \rho^{(1)} + \rho^{(2)} + \rho^{(3)} + \ldots$$

$P^3; S^{(3)}(t); \chi^{(3)}(\omega)$

4 Time domain response

$$S_{CARS} \sim \left| S^{(3)}(t_3, t_2, t_1) \right|^2$$

5

four time correlation functions

$$S^{(3)}(t) \Rightarrow \langle V(t_1)V(t_2)V(t_3)V(0) \rangle$$

$\Downarrow$ factorization of the Green functions

$\langle V(t)V(0) \rangle$ two time correlation functions

where

$$V = -\mu E \Rightarrow \begin{cases} \dfrac{\partial \mu}{\partial Q} \cdot Q \\ \dfrac{\partial \alpha}{\partial Q} \cdot Q \end{cases}$$

6 frequency domain response

$$S_{CARS} \sim \chi^{(3)} \left| (-\omega_s, \omega_1, \omega_2, \omega_3) \right|^2$$

$\Downarrow$ factorization

$$I(\omega_s) \cdot I(\omega_1) \cdot I(\omega_2)$$

$$\frac{1}{(\omega - \omega_1)^2 + \Gamma_1}$$

vibrational correlation function

$$\left\langle \frac{\partial \alpha(0)}{\partial Q} \cdot \frac{\partial \alpha(t)}{\partial Q} \right\rangle \langle Q(0) Q(t) \rangle$$

7 $$Q = Q_0 e^{-i(\omega_0 + \Delta\omega(t))t}$$

$\Downarrow$

8 $$Q = Q_0 \left\langle e^{-i(\Delta\omega(t))t} \right\rangle e^{-i\omega_0 t}$$

$\Downarrow$ cumulant expansion

$$e^{-i\int_0^t (\Delta\omega(0)\Delta\omega(t'))dt'}$$

$\Downarrow$

$$\Gamma = \frac{1}{2\pi c T_2} \Leftarrow T_2^{-1} = \left(T_2^{-1}\right)^* + \gamma^{-1}$$

band width — vibrational dephasing — pure dephasing — life time

NATIVE BR-568 AND UNLOCKED ANALOGS BR 6.11 AND 6.9

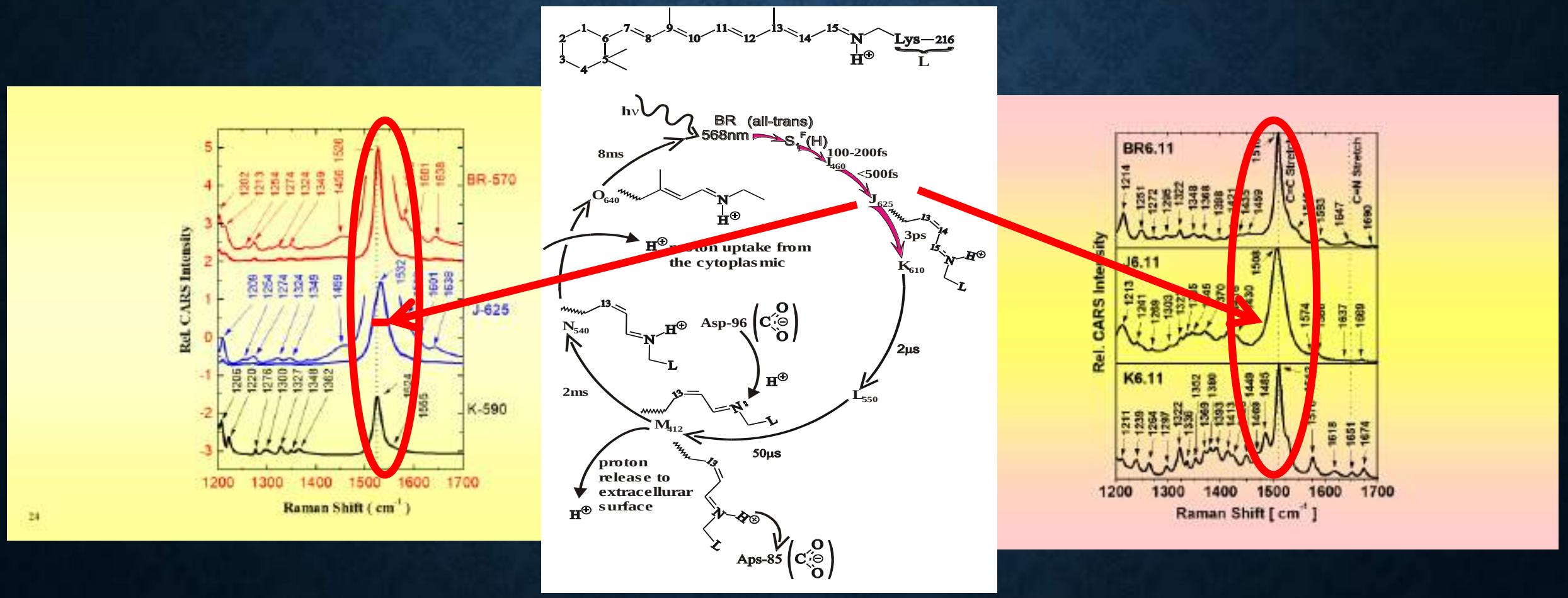

vibrational spectra of BR-570 (top), J-625 (center, derived from the 0-ps PTR/CARS data),and K-590 (bottom, derived from the 200-ps PTR/CARS data) in the1200–1700 cm1region

Locked analogs BR 5.12 and BR 5.13

BR 5.12

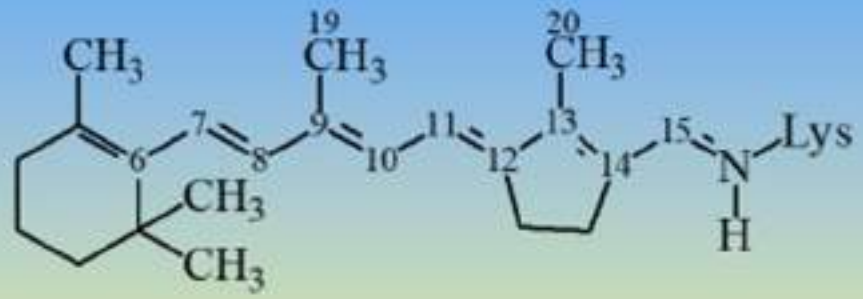

BR 5.13

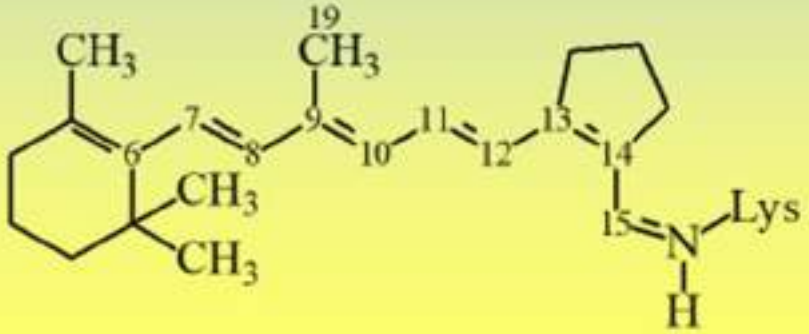

28

For BR5.12, the C13=C14 retinal bond is locked in the trans configuration by a rigid, five-membered carbon ring

Locked analogs BR 5.12 and BR 5.13

BR 5.12

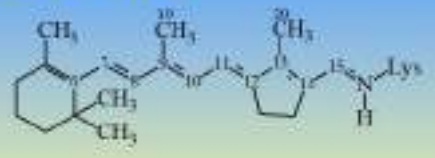

BR 5.13

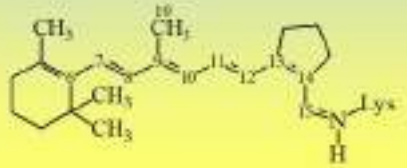

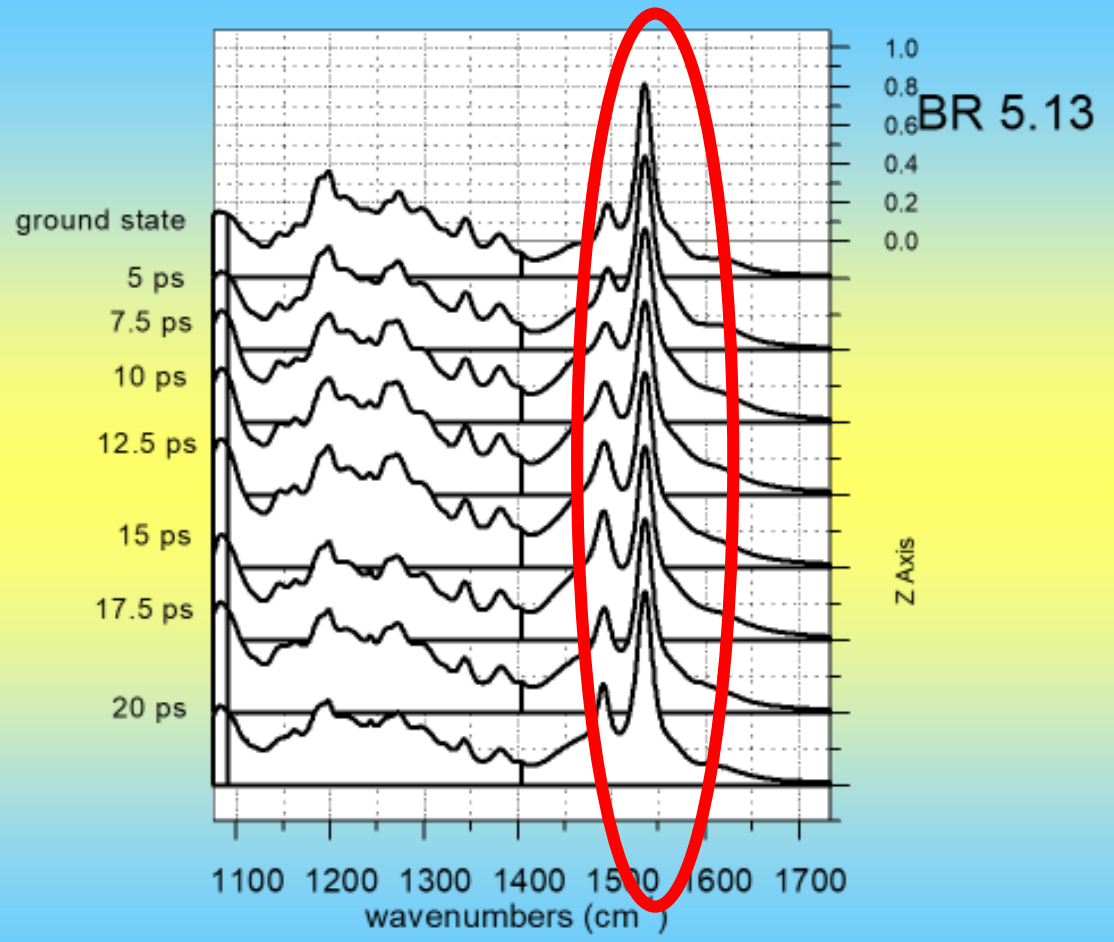

ELECTRONIC DYNAMICS OF BACTERIORHODOPSINE AND ITS MODIFIED ANALOGS

Excited state absorption

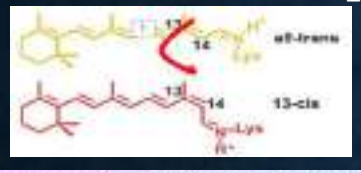

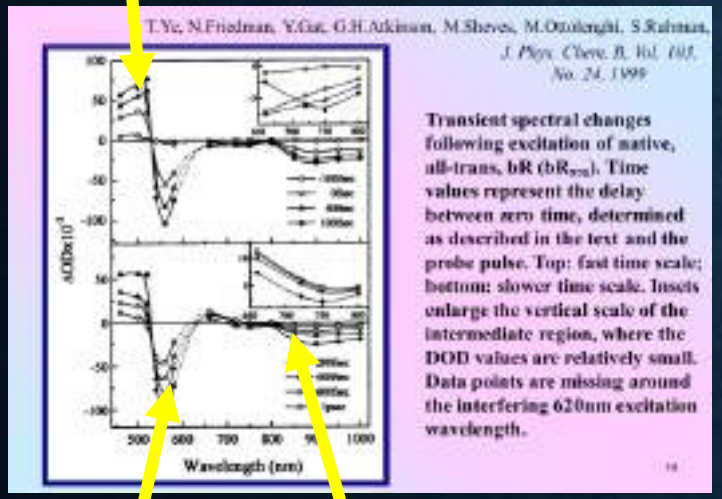

Stimulated emission

Ground state bleaching

Unanswered questions

- why the femtosecond spectra of native BR-568 and locked analogs are identical ?
- why the stimulated emission spectrum does not overlap with the spontaneous fluorescence?

The results demonstrated that the initial ultrafast spectral changes observed in native BR are virtually identical to those recorded for the modified analogs including a rise of the absorption/emission bands (460/860 nm) in less than 30 fs

Excited state absorption

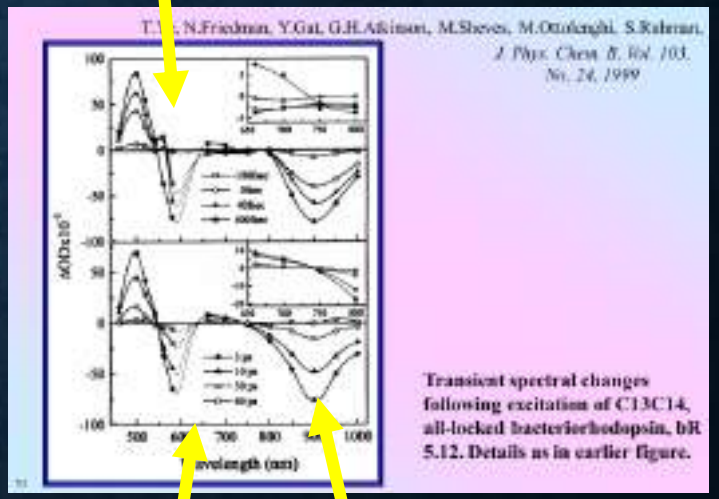

Ground state bleaching

Stimulated emission

LINEAR AND NONLINEAR RESPONSES VIBRATIONAL COUPLING THEORETICAL MODEL

$$I(\omega) = (2\pi)^{-1}\left[1-\exp\left(-\frac{\hbar\omega}{kT}\right)\right]\int_{-\infty}^{+\infty} dt e^{i\omega t}\left\langle M_{01}^{+}(0)M_{10}(t)\right\rangle$$

$$S_{IIB}(\omega_1\omega_2\tau) = \left(\frac{1}{\hbar}\right)^3 2\omega_2\int_0^\infty 2\omega_2\int_0^\infty dt_1\int_0^\infty dt_3\left[e^{i(\omega_1 t_1+\omega_2 t_3)}\chi(t_3+t_1)\left[R_1^{II}(t_3,\tau,t_1)+R_4^{II}(t_3,\tau,t_1)\right]\right]+$$
$$e^{i(\omega_2 t_3-\omega_1 t_1)}\chi(t_3-t_1)\left[R_2^{II}(t_3,\tau,t_1)+R_3^{II}(t_3,\tau,t_1)\right]$$

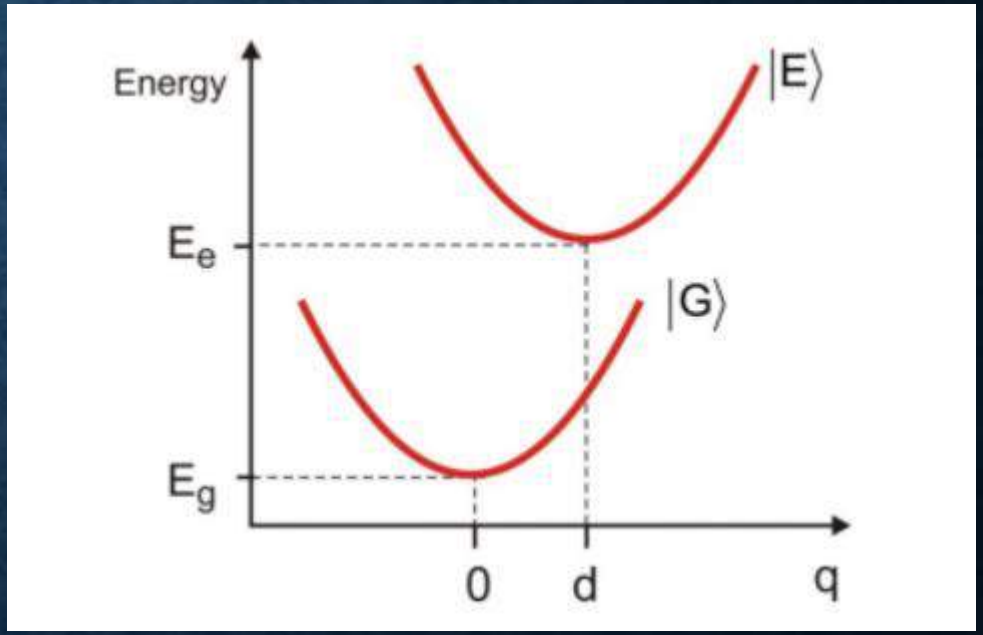

Shaul Mukamel Principles of Nonlinear Optical Spectroscopy

Molecular excited states have geometries that are different from the ground state configuration as a result of varying electron configuration. This parametric dependence of electronic energy on nuclear configuration results in a variation of the electronic energy gap between states as one stretches bond vibrations of the molecule. We are interested in describing how this effect influences the electronic absorption spectrum, and thereby gain insight into how one experimentally determines the coupling of between electronic and nuclear degrees of freedom. We consider electronic transitions between bound potential energy surfaces for a ground and excited state as we displace a nuclear coordinate q. The simplified model consists of two harmonic oscillators potentials whose 0-0 energy splitting is $E_e - E_g$ and which depends on q. We will calculate the absorption spectrum in the interaction picture using the time-correlation function for the dipole operator.

HOLE BURNING PROFILES

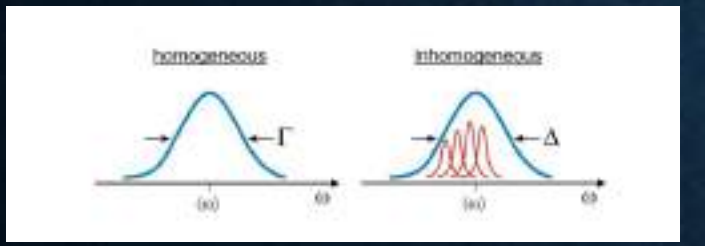

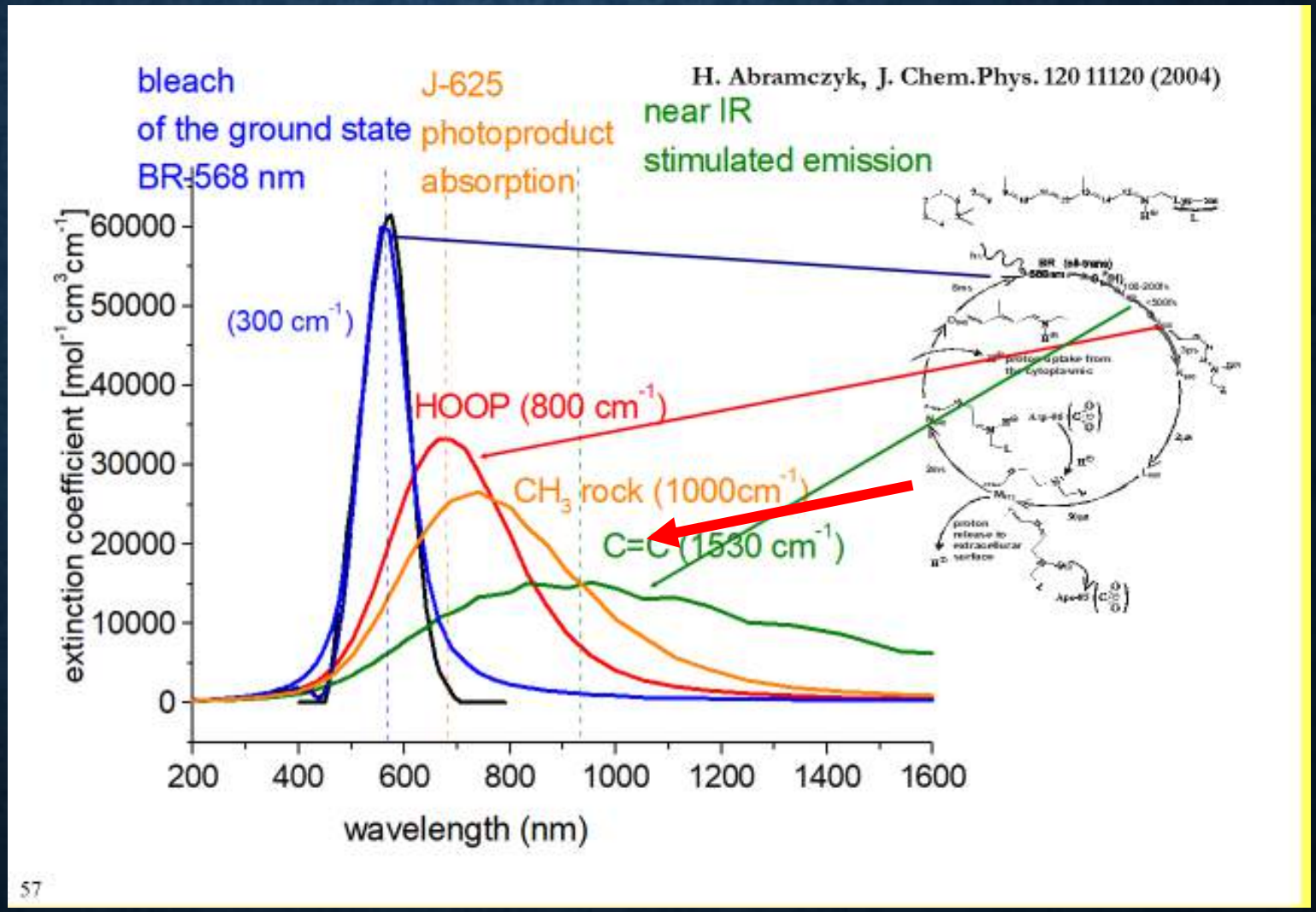

the high frequency mode (C=C stretching), not the torsional coordinate, i the primary accepting mode

H. Abramczyk, Femtosecond primary events in bacteriorhodopsin. Revision of commonly accepted interpretation of electronic spectra of transient intermediates, J. Chem. Phys. 120 11120 (2004)

PREVIOUS MODELS

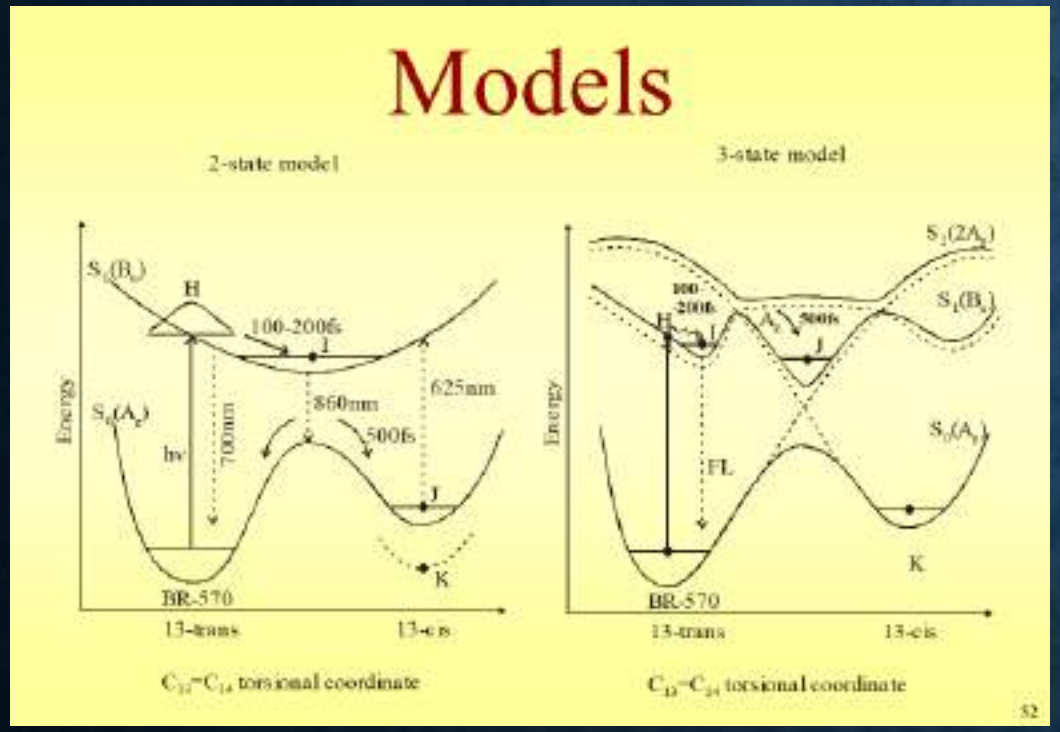

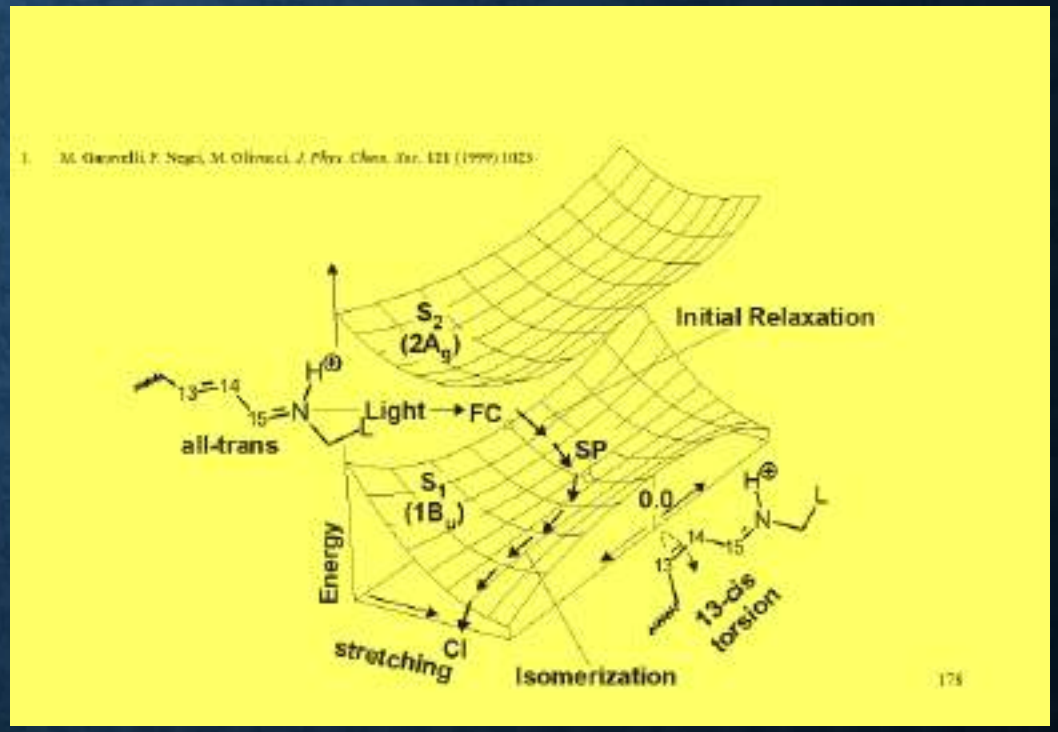

Despite the great diversity of traditional and modern approaches of experimental and theoretical methods applied to study the family of rhodopsins , which are responsible for vision processes, there is no generally accepted view on ultrafast primary events

CONCLUSIONS-1

PROPOSED MECHANISM OF PRIMARY EVENTS IN BR PHOTOCYCLE

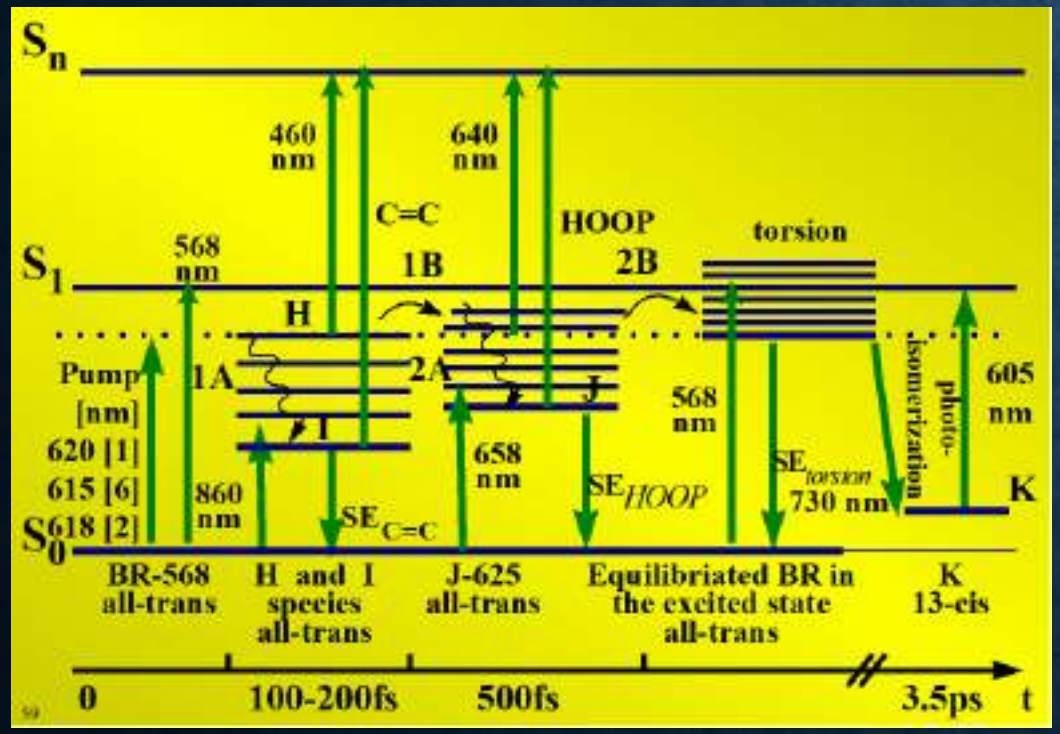

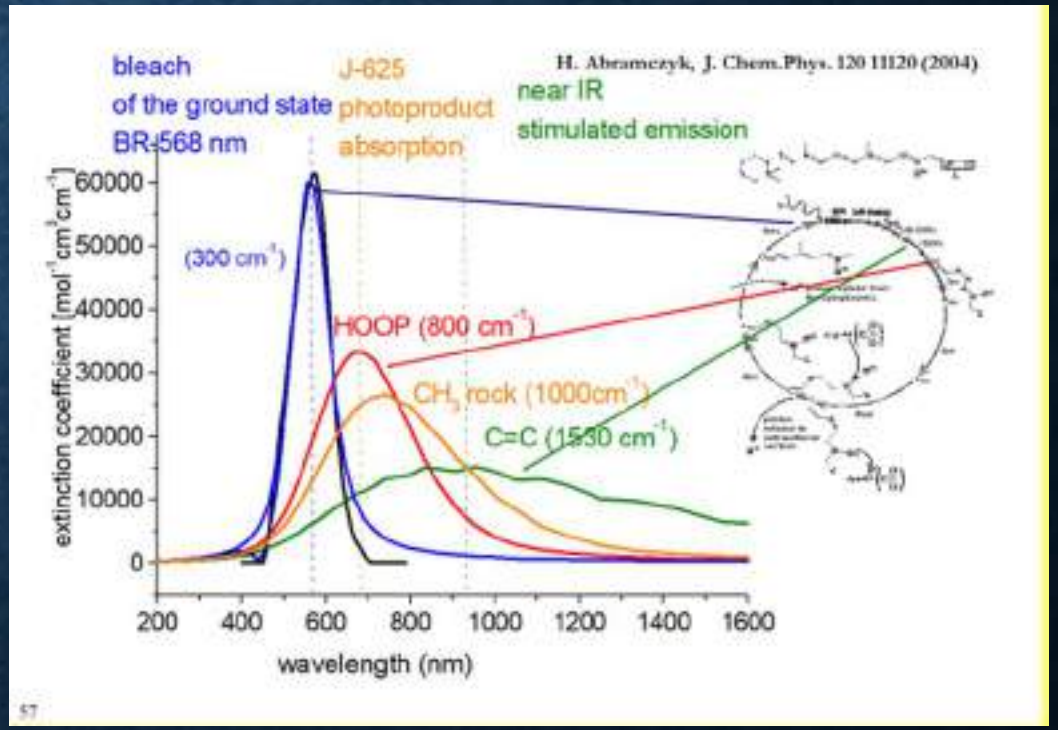

H. Abramczyk, Femtosecond primary events in bacteriorhodopsin. Revision of commonly accepted interpretation of electronic spectra of transient intermediates, J. Chem. Phys. 120 11120 (2004)

FREE RETINOIDS AND RETINOIDS BOUND TO PROTEINS

Is femtosecond dynamics of retinoids ,,free'' in solution different from that in retinoids bound to proteins?

Answering this question is very important , because femtosecond dynamics could monitor free retinol and retinol bound to proteins in cells providing information on the mechanism of retinol uptake and signalling by STRA6

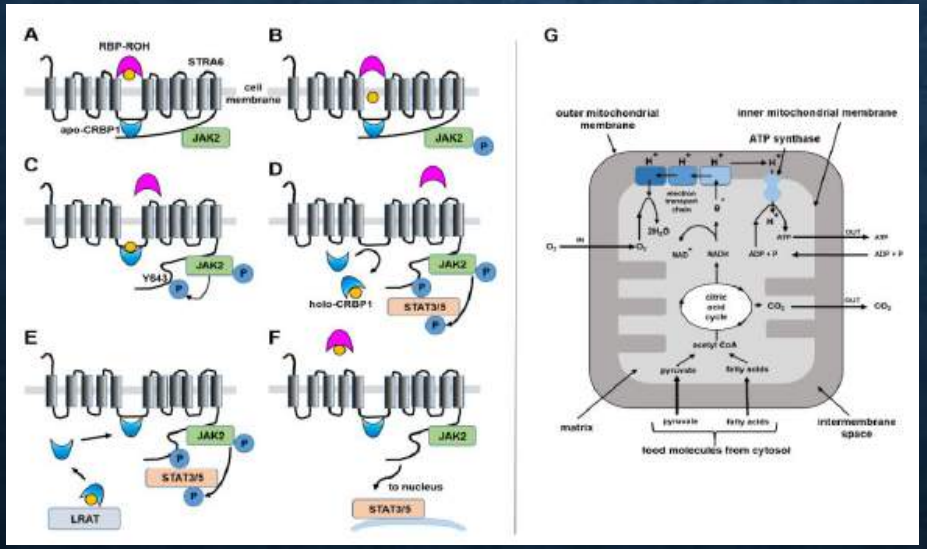

Model of the mechanism of retinol uptake and signalling by STRA6

RETINOIDS FREE IN SOLUTIONS

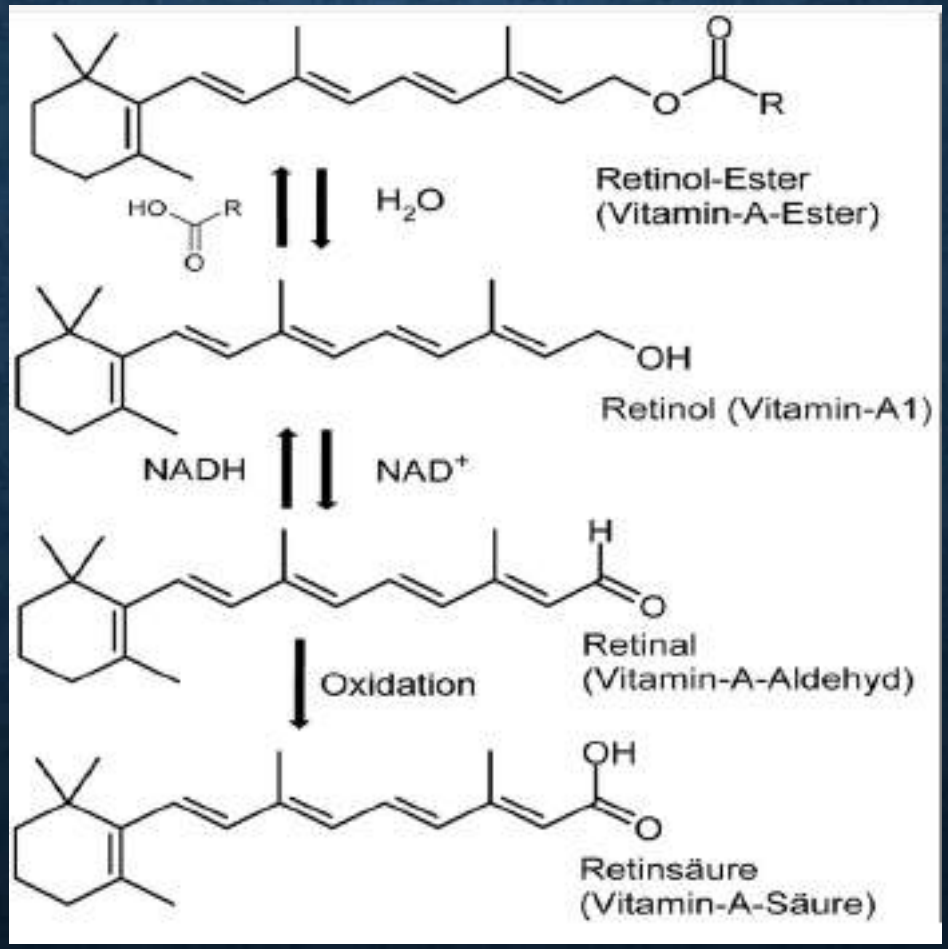

PUMP-PROBE TRANSIENT ABSORPTION FEMTOSECOND SPECTROSCOPY

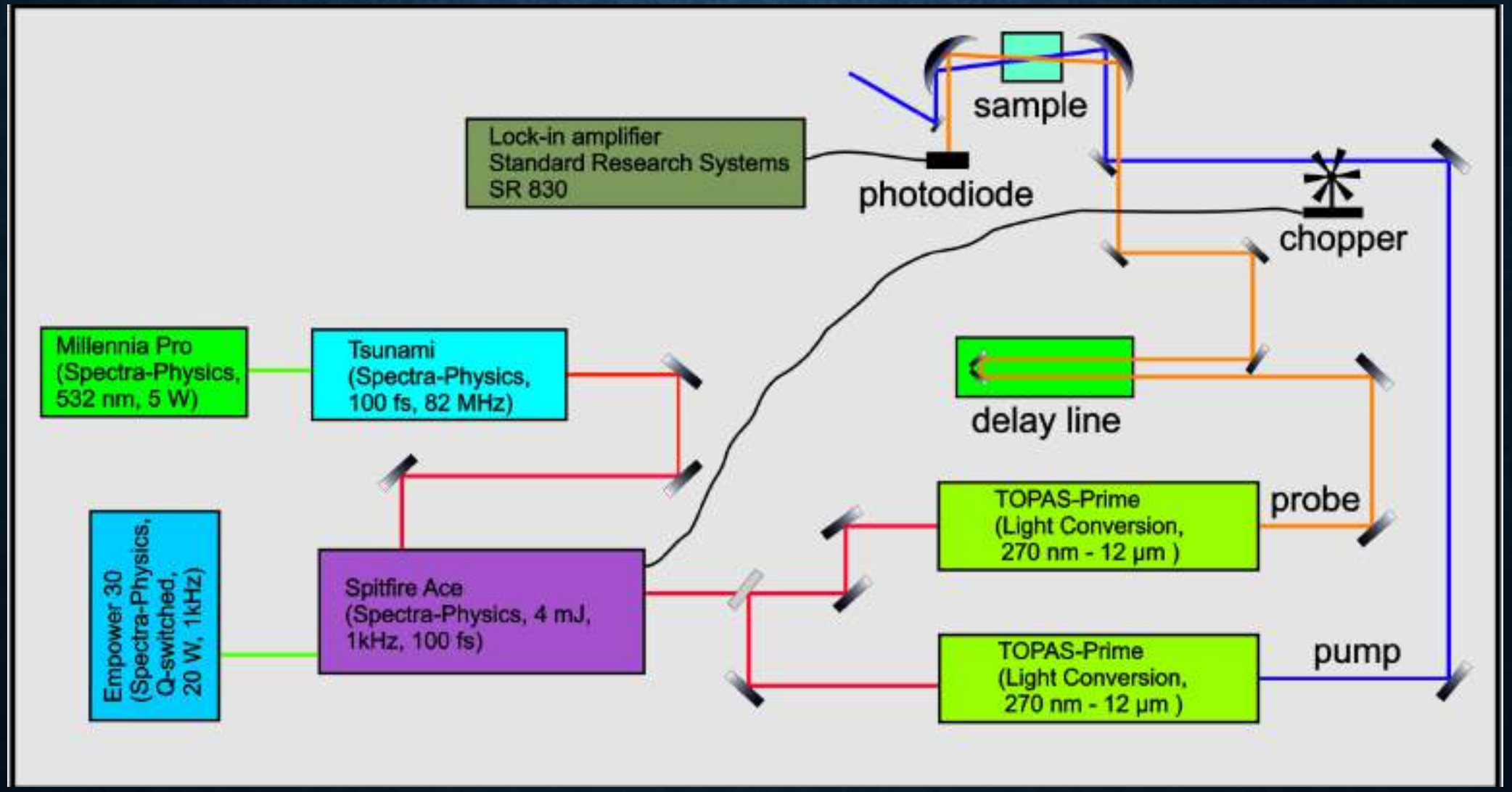

PUMP-PROBE TRANSIENT ABSORPTION FEMTOSECOND SPECTROSCOPY

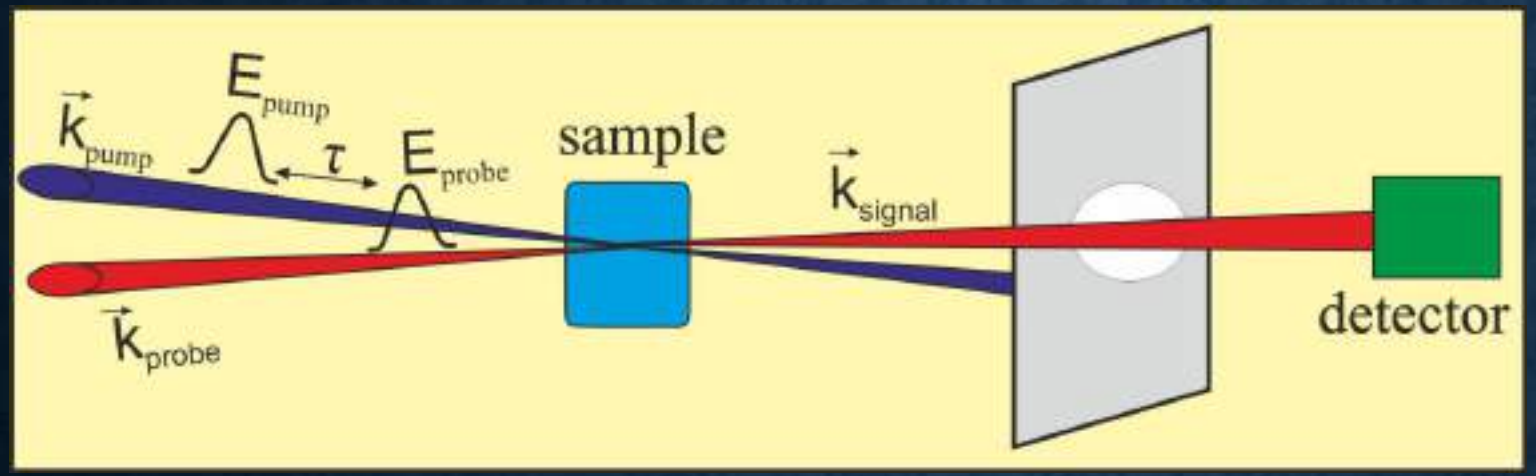

the measured pump-probe signal is proportional to the imaginary part of the polarization

$$\Delta I(\tau) = 2\omega_{sig}\ell \,\mathrm{Im}\left[E'_{pr}P^{(3)}(\tau)\right]$$

The pump-probe or transient absorption experiment is perhaps the most widely used third-order nonlinear experiment. It can be used to follow many types of time-dependent relaxation processes and chemical dynamics, and is most commonly used to follow population relaxation, chemical kinetics, or wavepacket dynamics and quantum beats.

PUMP-PROBE TRANSIENT ABSORPTION FEMTOSECOND SPECTROSCOPY

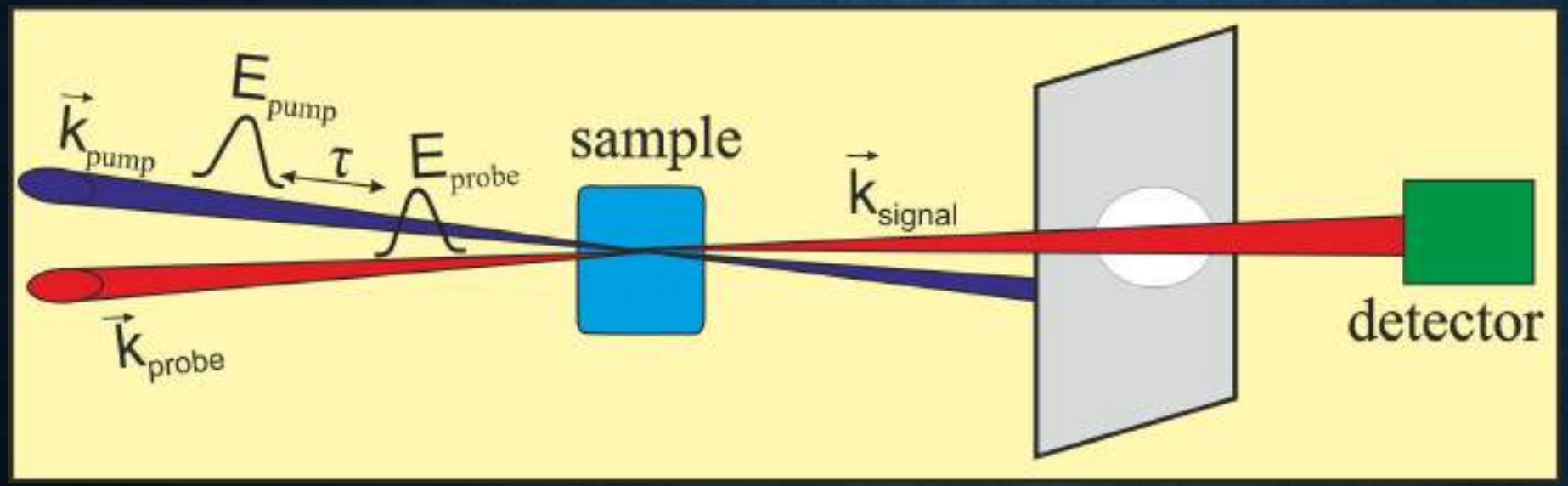

the measured pump-probe signal is proportional to the imaginary part of the polarization

$$\Delta I(\tau) = 2\omega_{sig}\ell \,\mathrm{Im}\left[E'_{pr}P^{(3)}(\tau)\right]$$

The principle is quite simple: two pulses separated by a delay τ are crossed in a sample: a pump pulse and a time-delayed probe pulse. The pump pulse Epu creates a non-equilibrium state, and the time-dependent changes in the sample are characterized by the probe-pulse Epr through the pump-induced intensity change on the transmitted probe, ΔI.

GROUND STATE BLEACHING OF RETINOIDS IN SOLUTION (N-HEXANE, MAGIC ANGLE)

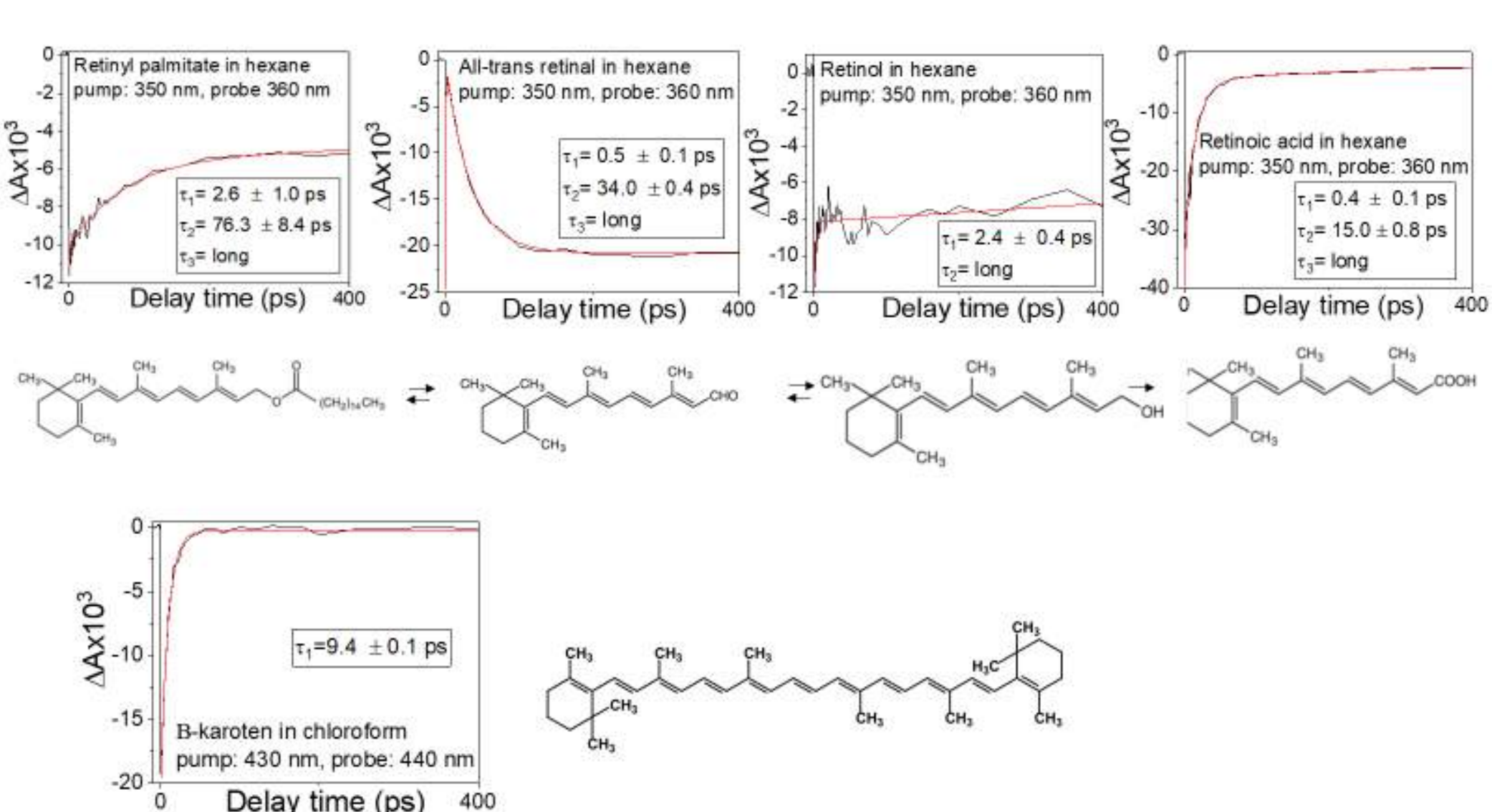

GROUND STATE BLEACHING OF RETINOIDS IN SOLUTION (CHLOROFORM)

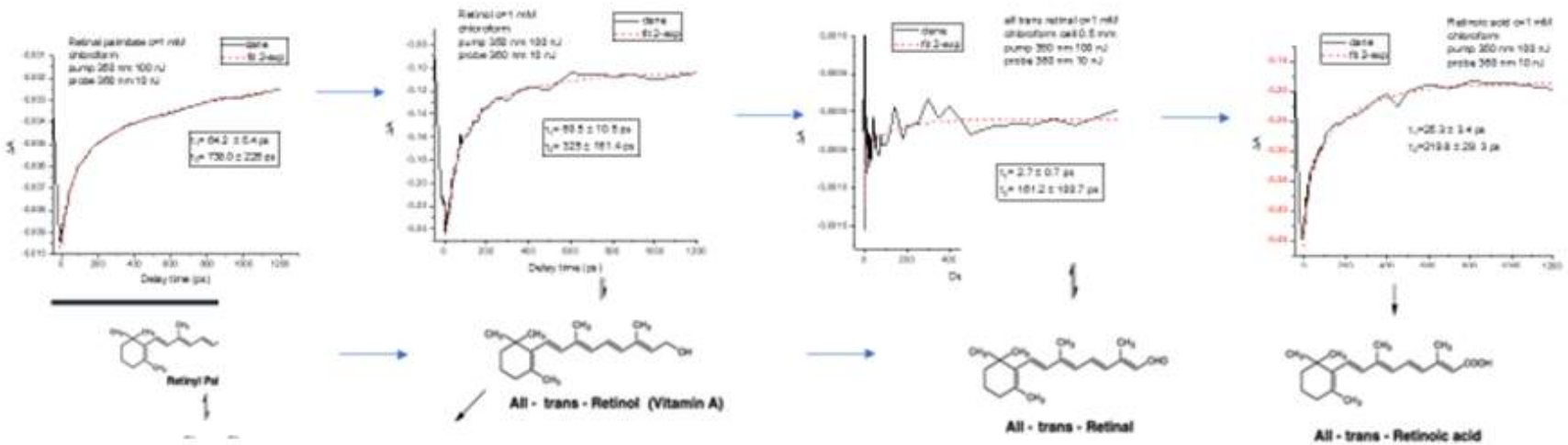

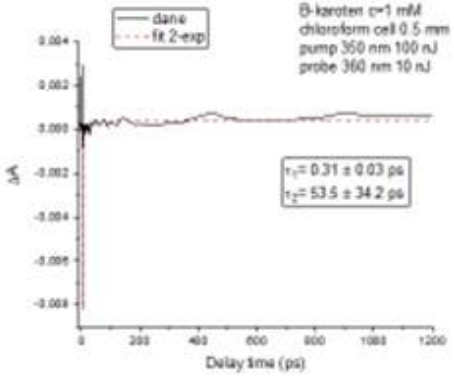

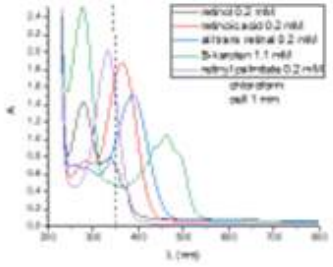

Pump 350 nm 100 nJ
Probe 360 nm 10 nJ

	t1	t2
B-karoten	0.31 ± 0.03 ps	53.5 ± 34.2 ps
Retinyl palmitate	64.2 ± 5.4 ps	738.0 ± 226 ps
All trans-retinal	2.7 ± 0.7 ps	161.2 ± 100.7 ps
Retinoic acid	25.3 ± 3.4 ps	219.8 ± 29. 3 ps
retinol	60.5 ± 10.5 ps	325 ± 161.4 ps

EXCITED STATE ABSORPTION OF RETINOIDS IN SOLUTION (N-HEXANE, MAGIC ANGLE)

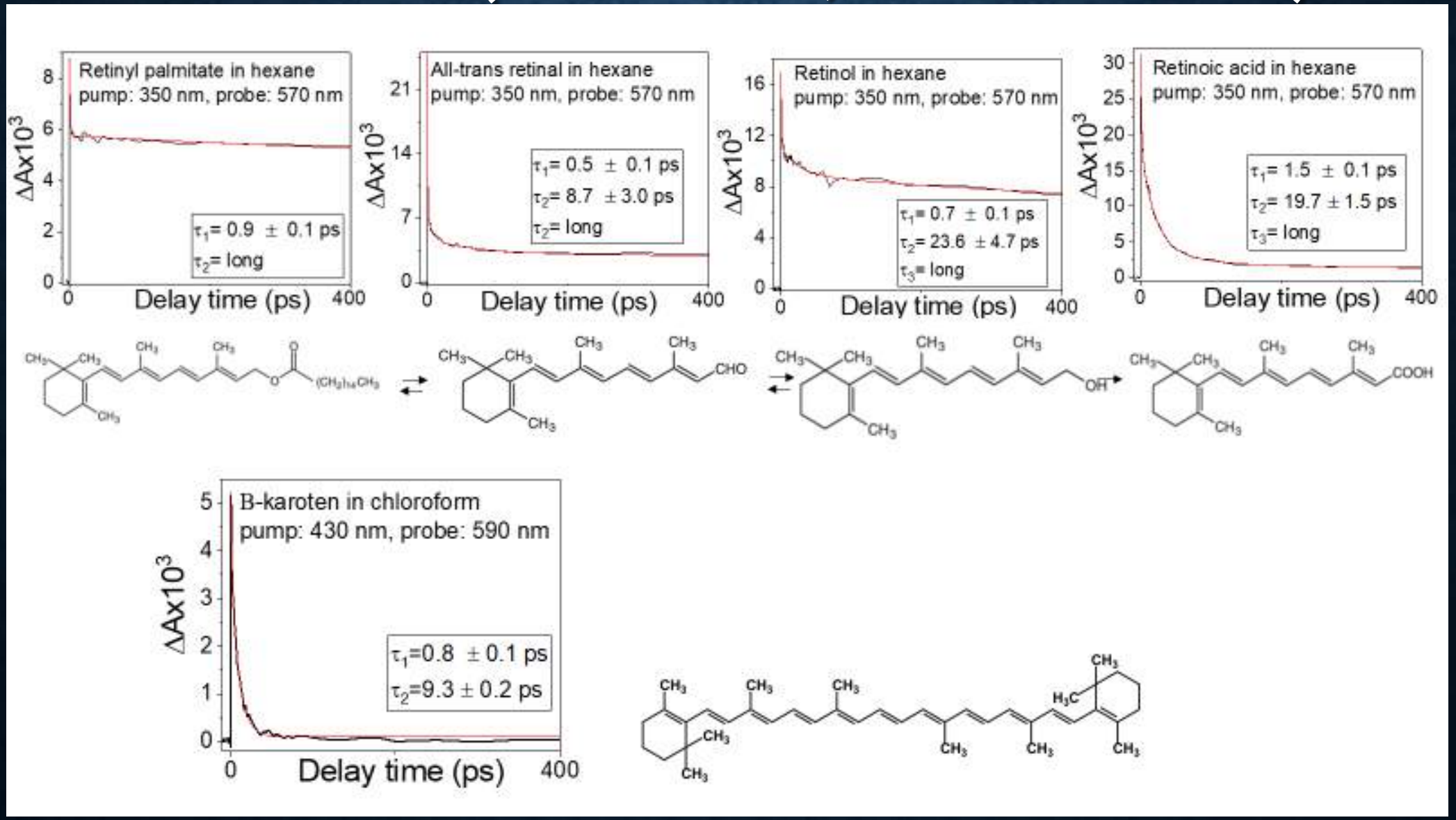

EXCITED STATE ABSORPTION OF RETINOIDS IN SOLUTION (CHLOROFORM)

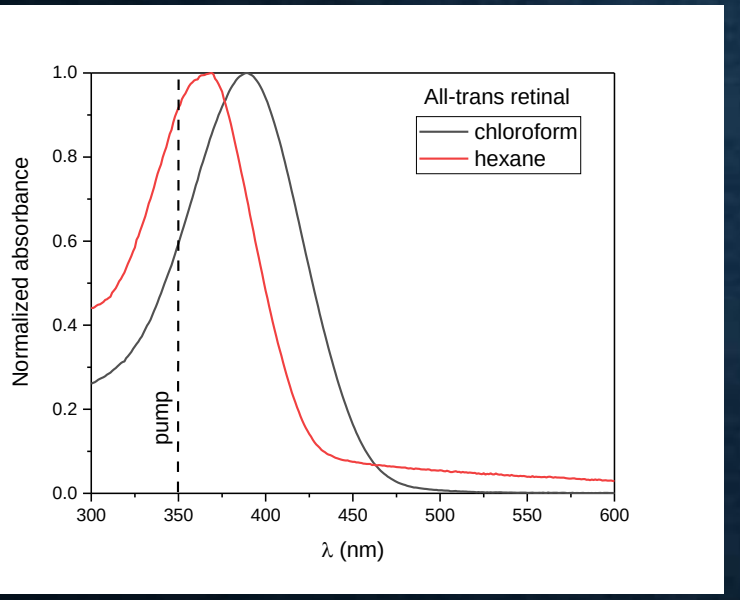

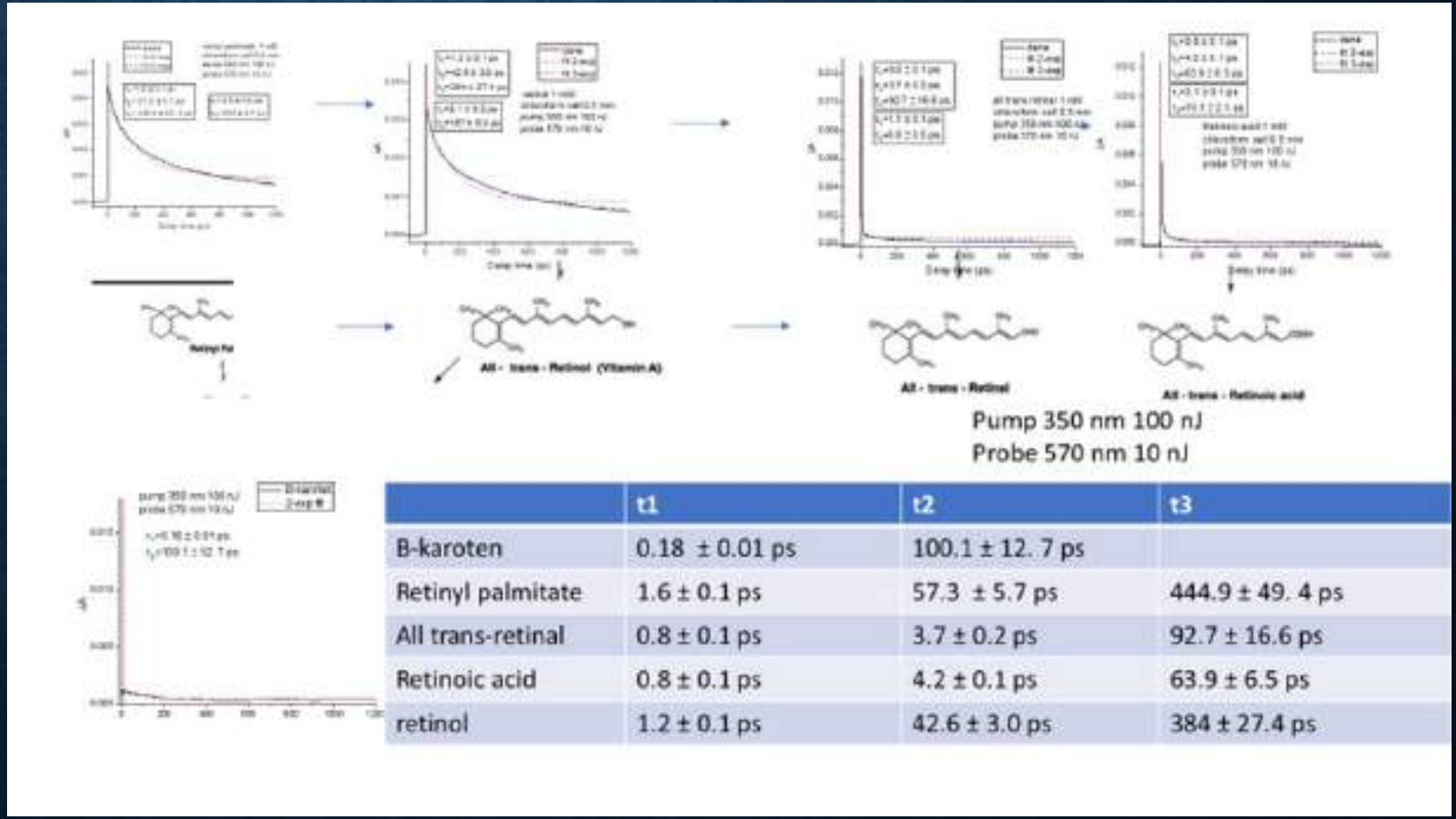

	t1	t2	t3
B-karoten	0.18 ± 0.01 ps	100.1 ± 12. 7 ps	
Retinyl palmitate	1.6 ± 0.1 ps	57.3 ± 5.7 ps	444.9 ± 49. 4 ps
All trans-retinal	0.8 ± 0.1 ps	3.7 ± 0.2 ps	92.7 ± 16.6 ps
Retinoic acid	0.8 ± 0.1 ps	4.2 ± 0.1 ps	63.9 ± 6.5 ps
retinol	1.2 ± 0.1 ps	42.6 ± 3.0 ps	384 ± 27.4 ps

B–CAROTENE

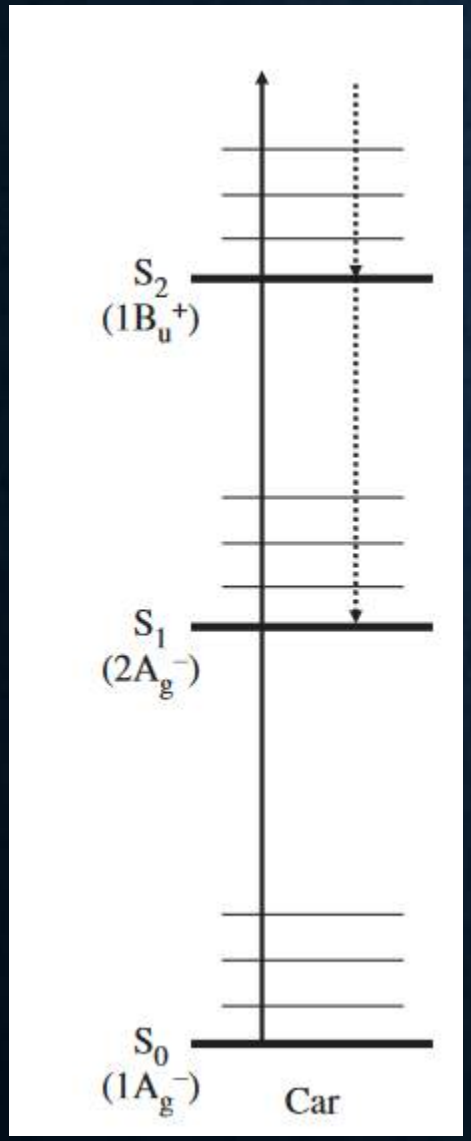

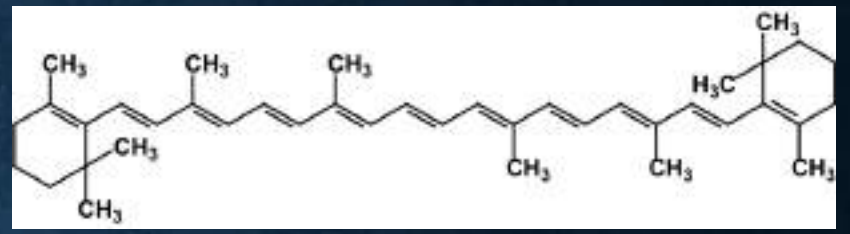

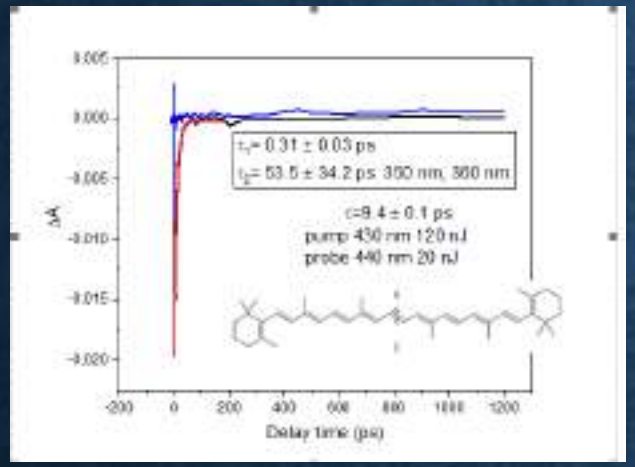

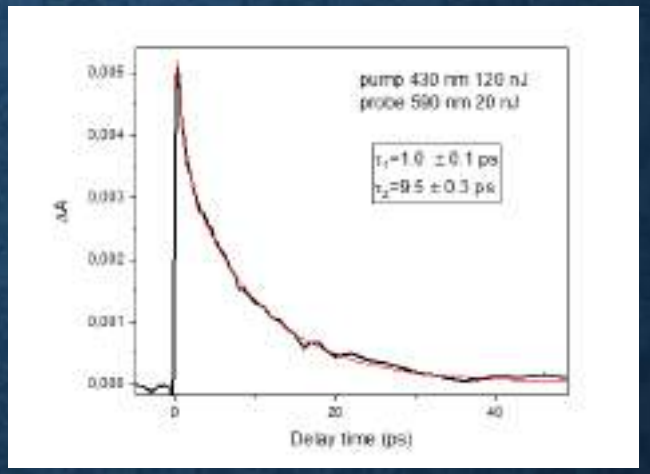

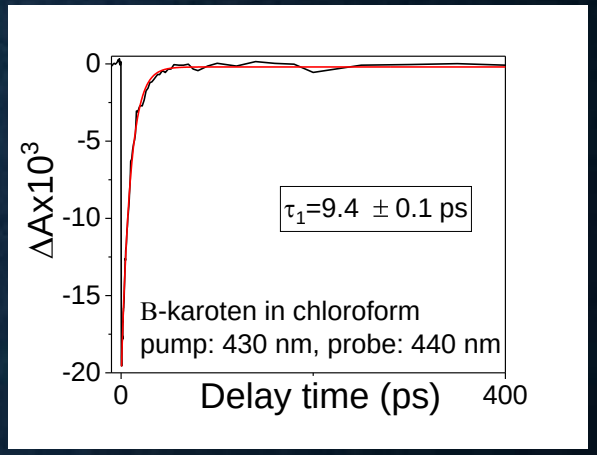

The bleaching results correspond well to the excited state absorption (ESA) of the S1 state shown in Figure. The ESA rises immediately the excitation and decays biexponentially with the times of 1 and 9.5 ps. The first one reflects vibrational relaxation in S1 state, the 9.5 ps reflects the decay to the S0 state corresponding perfectly to the lifetime of S0 state recovery within 9.4 ps.

ALL-TRANS RETINAL

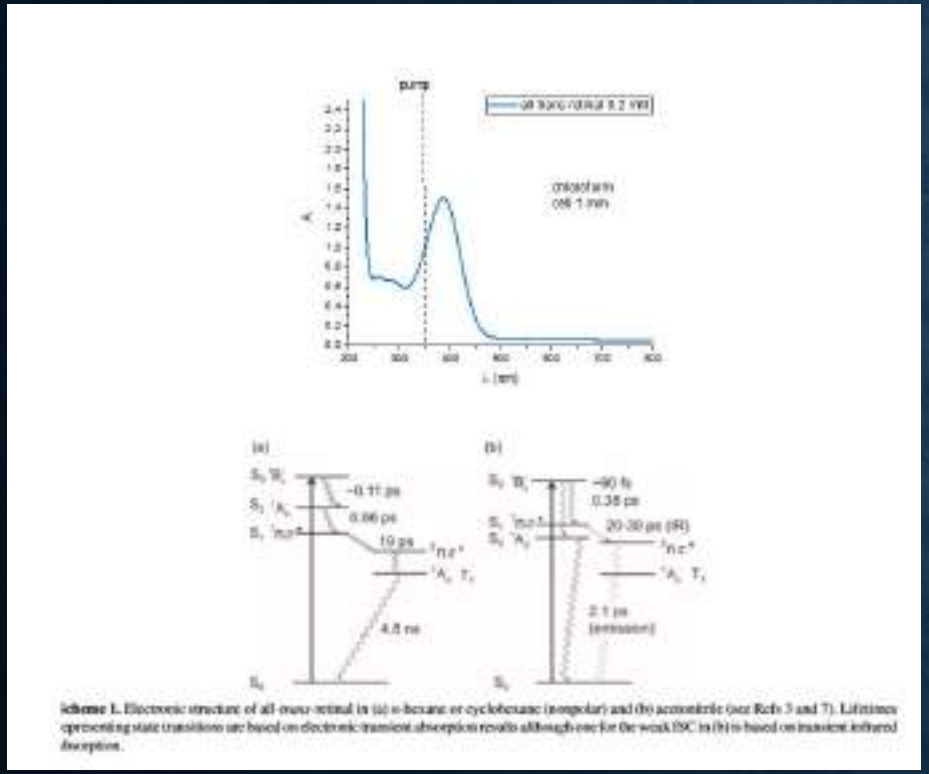

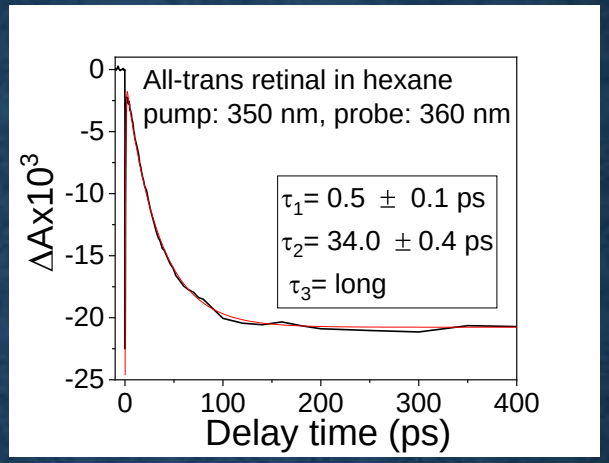

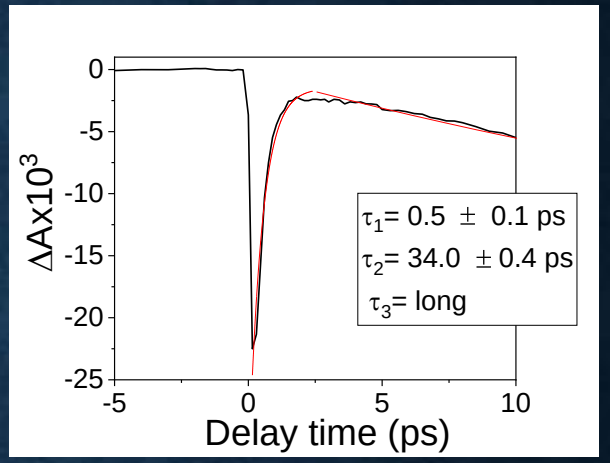

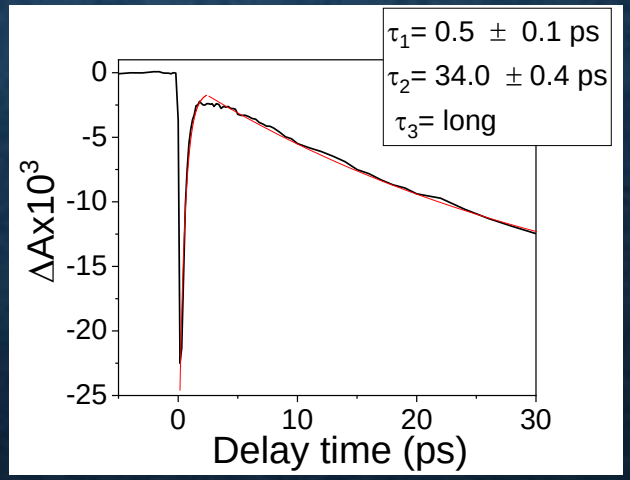

Fig. 7 shows the electronic structure levels for all-trans retinal . It consists of three excited singlet states in the near -UV-visible spectral region (Fig.2). The excited states S_2 $A_g(\pi\pi^*)$ and S_3 $B_u(\pi\pi^*)$ represent a polyene electronic structure, $S_1(n\pi^*)$ represents the aldehyde group of all-trans retinal.

ALL-TRANS RETINOL

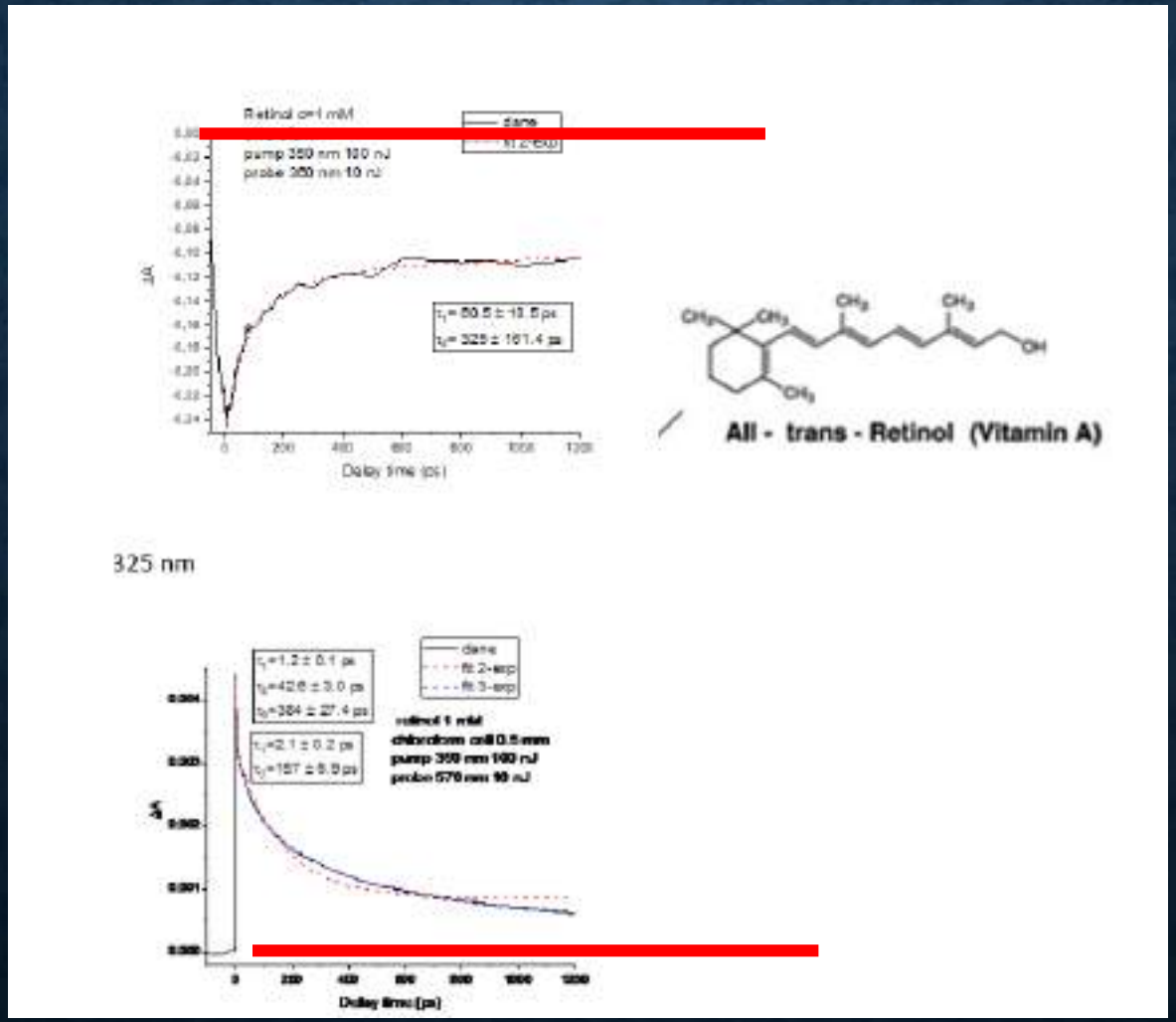

ULTRAFAST DYNAMICS OF METAL COMPLEXES OF TETRASULPHONATED PHTHALOCYANINES AT BIOLOGICAL INTERFACES OF THE HUMAN TISSUE

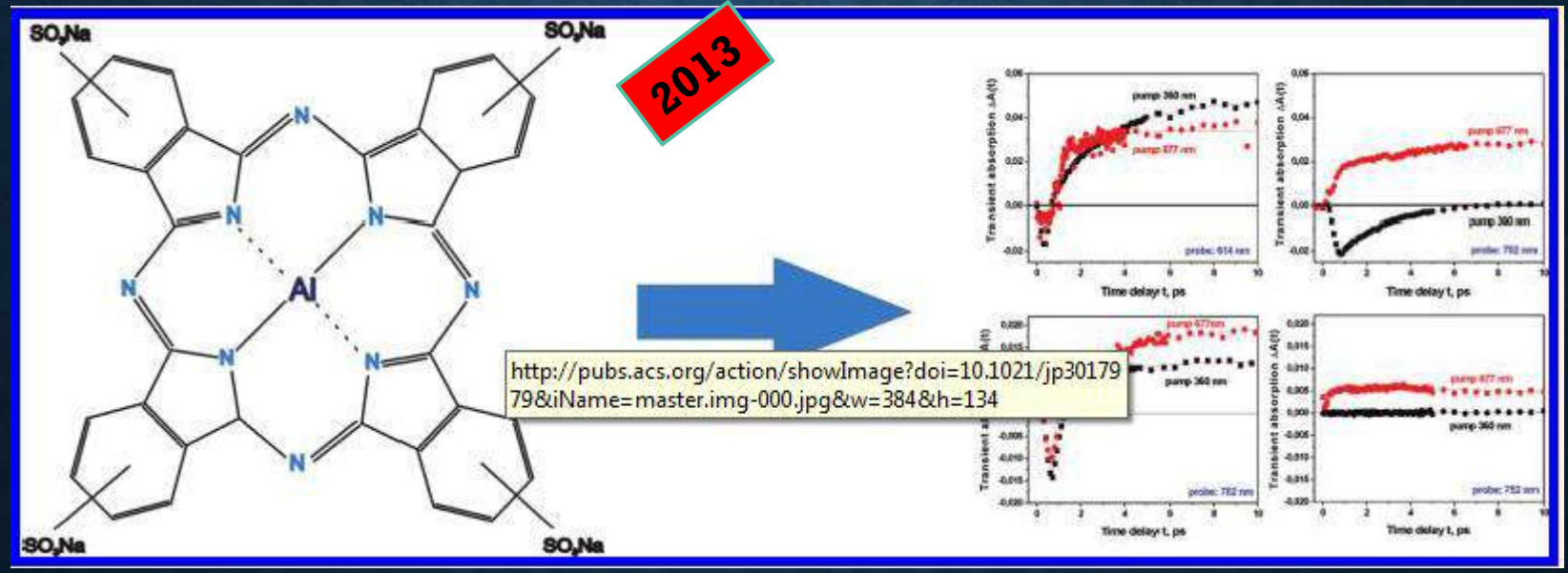

Arkadiusz Jarota, Marc Tondusson, Geoffrey Galle,Eric Freysz, and Halina Abramczyk , 2012

THE JOURNAL OF PHYSICAL CHEMISTRY A

Femtosecond spectroscopy of human breast tissues with aluminum phthalocyanine

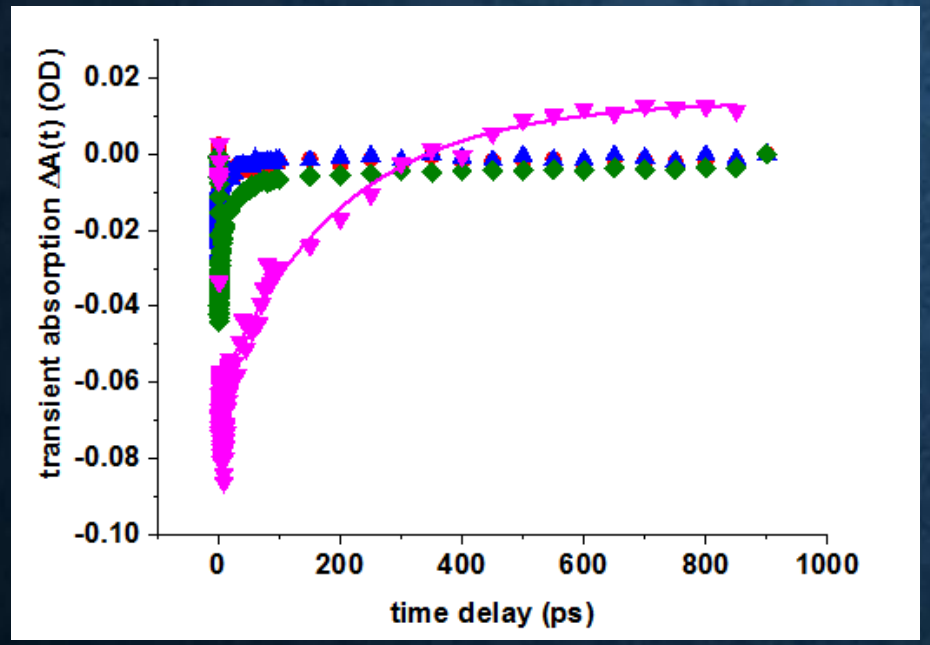

pump 677 nm, probe 670 nm
P58

Normal tissue
130 ± 0.10 fs, 1.53 ± 0.19 ps, i 37.86 ± 5.25 ps Cancer tissue
110±0.10 fs, 1.34±0.16 ps, i 40.72±7.86 ps
Film
830±100 fs, 7.31±1.02 ps, i 56.03±6.58 ps
Solutions
232.52±81.00 ps, 5.09 ± 0.99 ps

H. Abramczyk, B. Brozek-Pluska, E. Freysz, M. Tondusson, *J. Phys. Chem. C* 2013, 113, 4999.

Femtosecond spectroscopy of human breast tissues with aluminum phthalocyanine

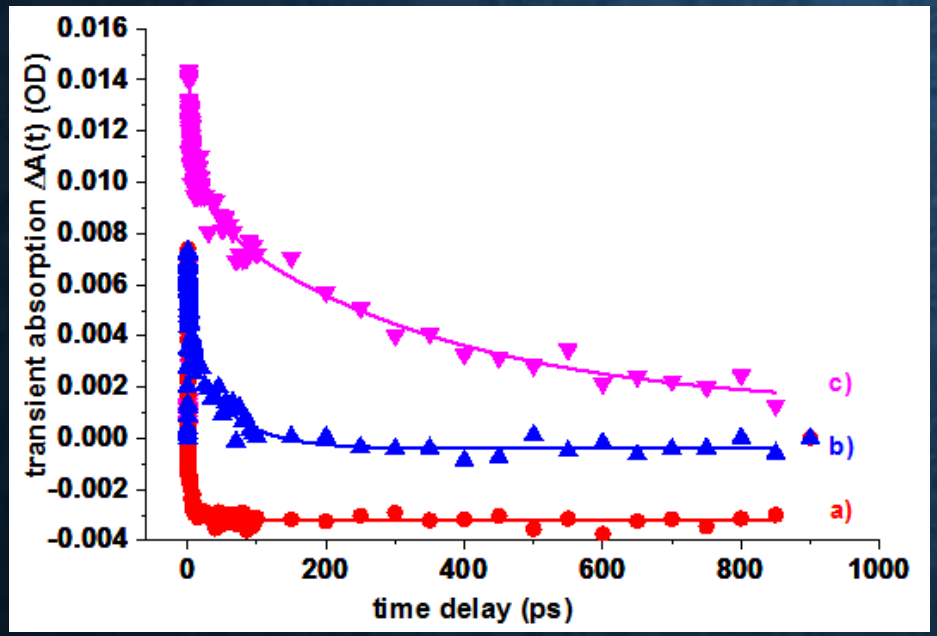

pump 677 nm, probe 602 nm
P58

Cancer tissue
810±0.0.04 fs, 5.63±0.49 ps, i 59.90±1.85 ps
Normal tissue
176 ± 0.20 fs, 840 ± 0.42 fs, i 6.03 ± 1.92 ps
Solutions
345.81±107.00 ps, 2.37 ± 0.71 ps

H. Abramczyk, B. Brozek-Pluska, E. Freysz, M. Tondusson,
J. Phys. Chem. C 2013, 113, 4999.

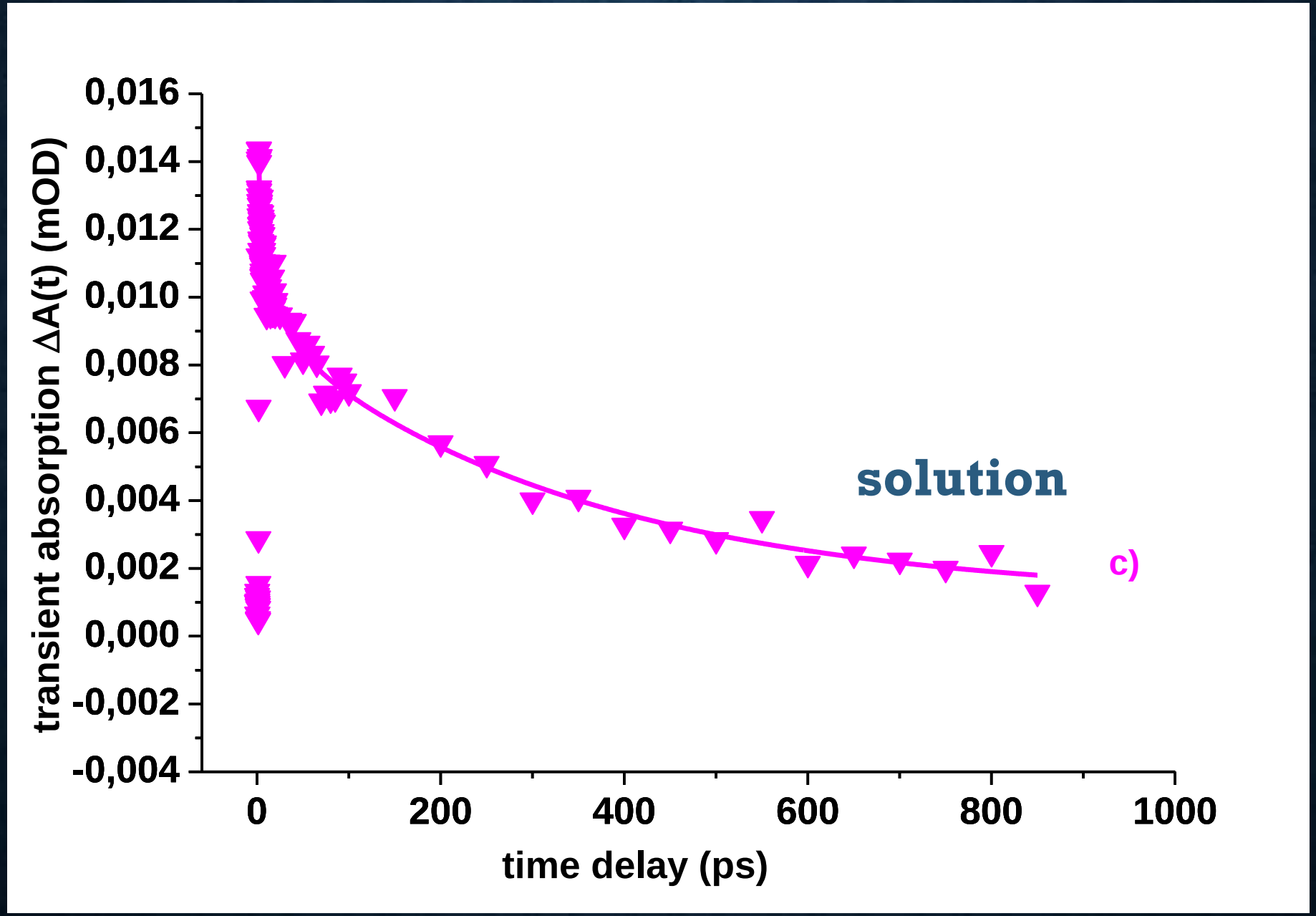

the results showed that the dynamics of the photosensitizer was markedly faster in the interfacial regions of the biological tissue than in solutions. Second, the photosensitizer localized in noncancerous tissue dissipates the energy through different pathways than that in cancerous breast tissue.

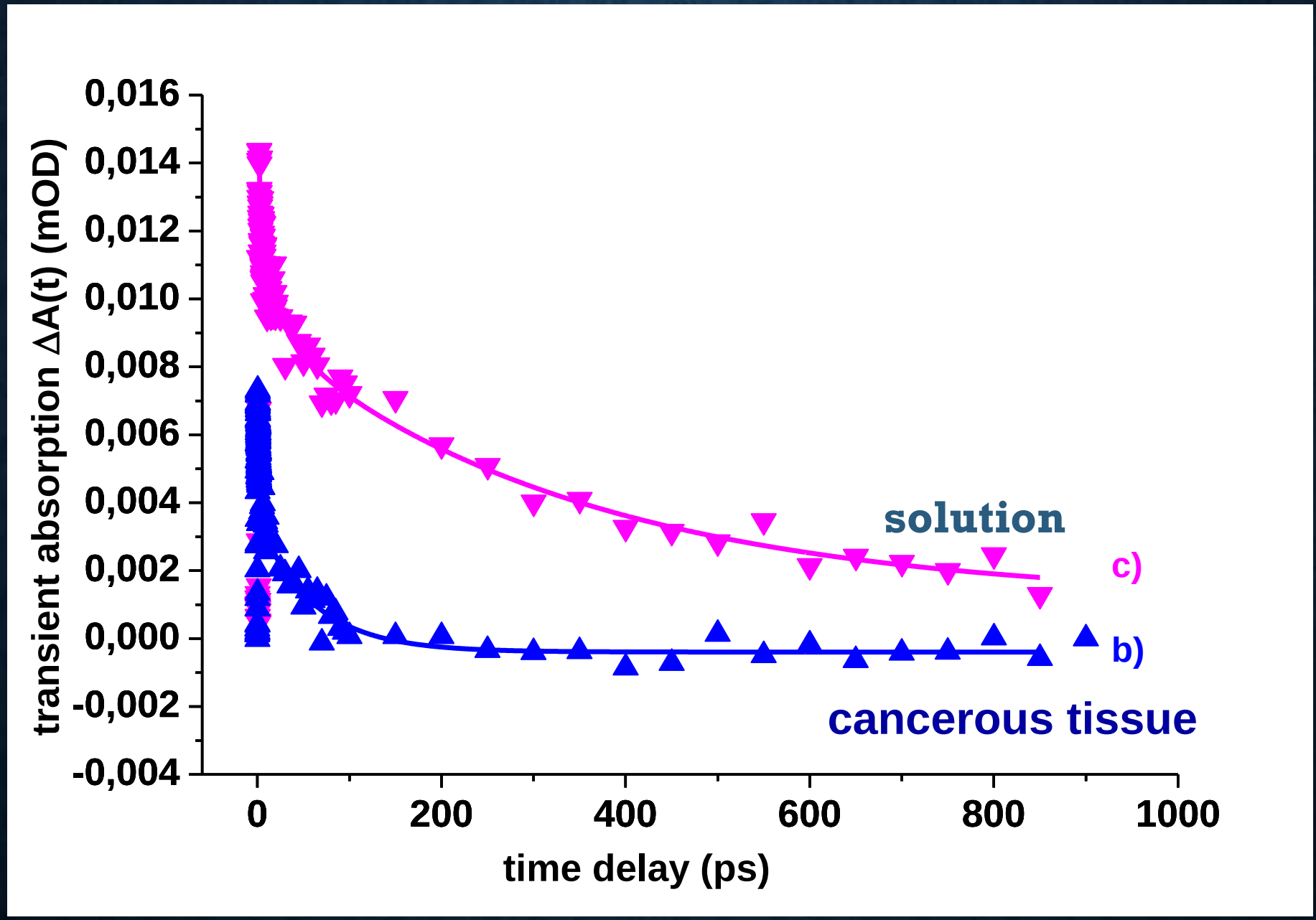

the results showed that the dynamics of the photosensitizer was markedly faster in the interfacial regions of the biological tissue than in solutions. Second, the photosensitizer localized in noncancerous tissue dissipates the energy through different pathways than that in cancerous breast tissue.

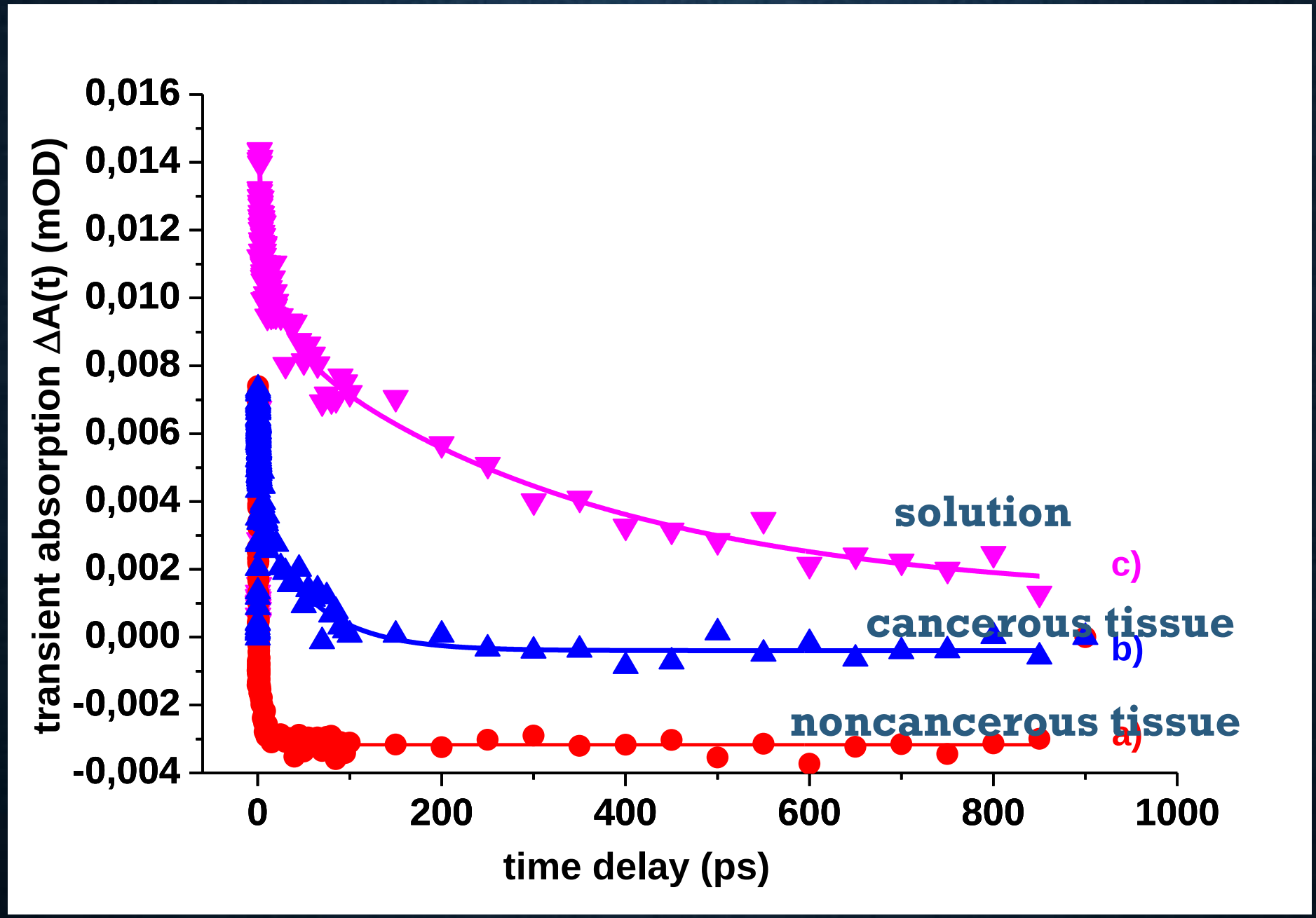

We have shown that the lifetimes characterizing both the ground state S_0 and the first excited state S_1 in the interfacial regions of noncancerous tissue are markedly shorter than those in cancerous tissue.

RAMAN SPECTRA OF RETINOIDS

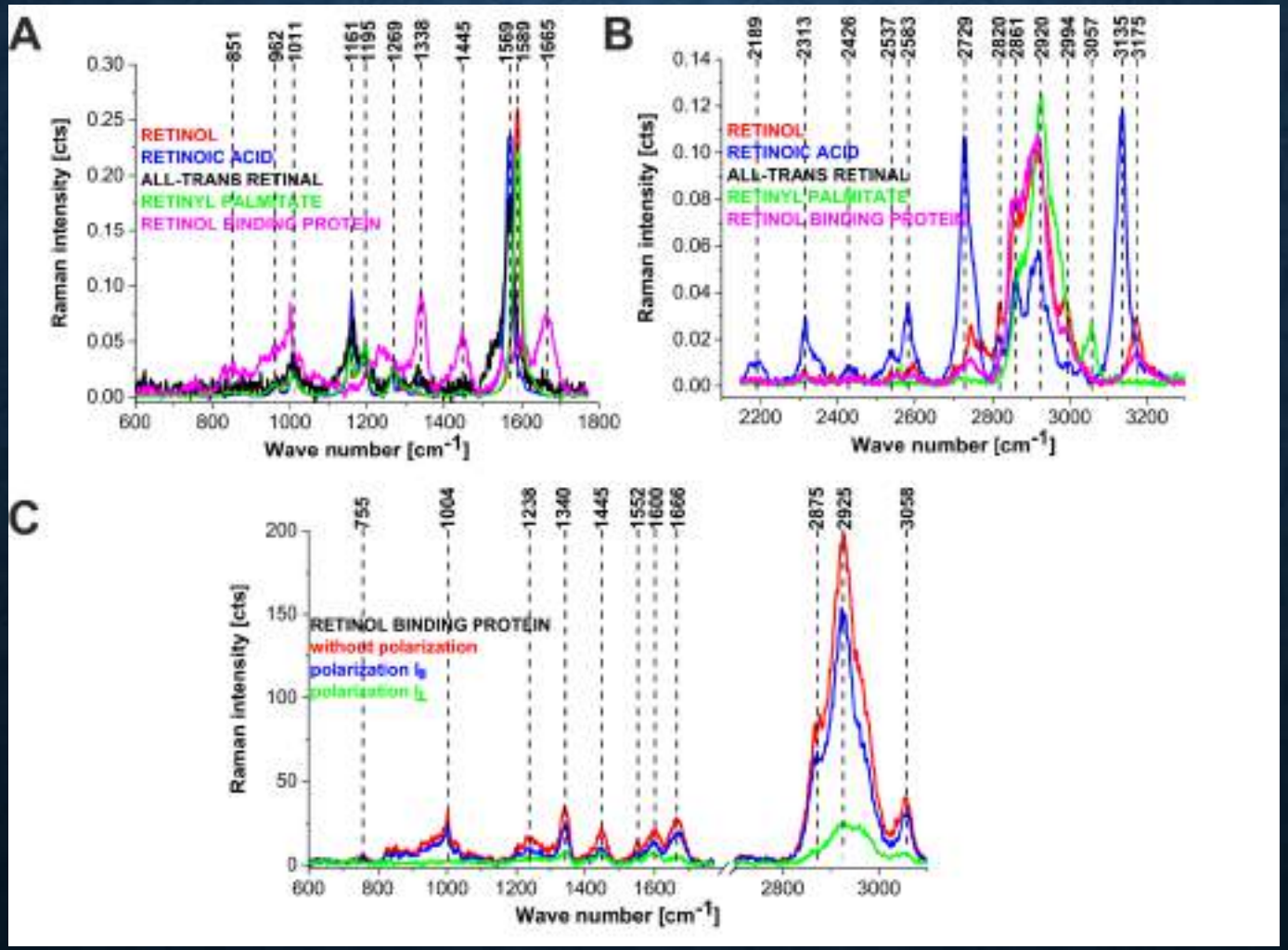

METHODS OF MOLECULAR AND LASER MICROSPECTROSCOPY IMAGING

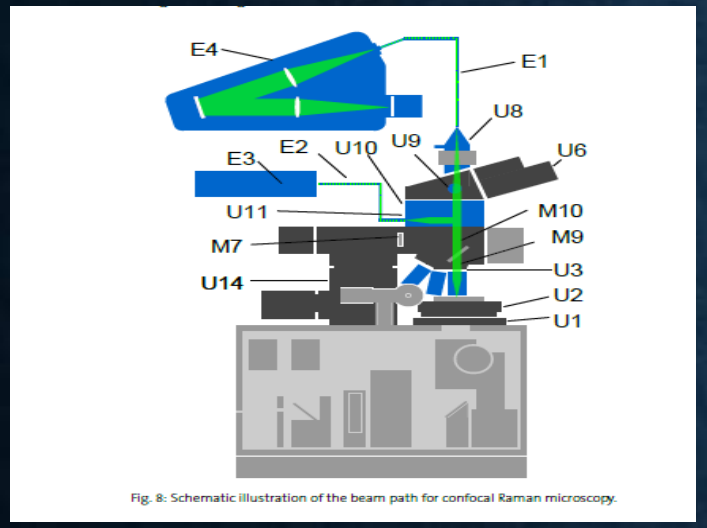

Fig. 8: Schematic illustration of the beam path for confocal Raman microscopy.

Raman imaging

IR imaging

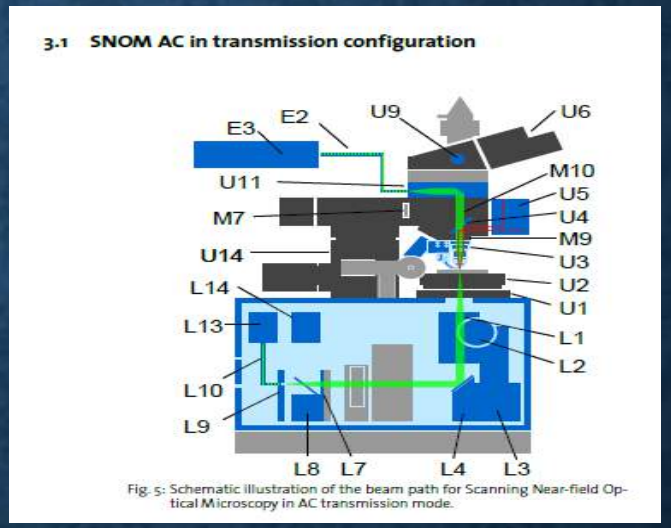

Fig. 5: Schematic illustration of the beam path for Scanning Near-field Optical Microscopy in AC transmission mode.

SNOM imaging

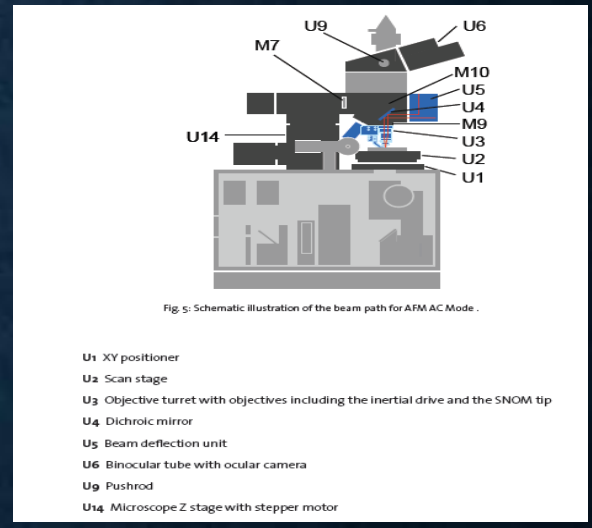

Fig. 5: Schematic illustration of the beam path for AFM AC Mode .

AFM imaging

We do not need to disrupt cells to break open the cells and release the cellular structures

CONVENTIONAL MOLECULAR BIOLOGY

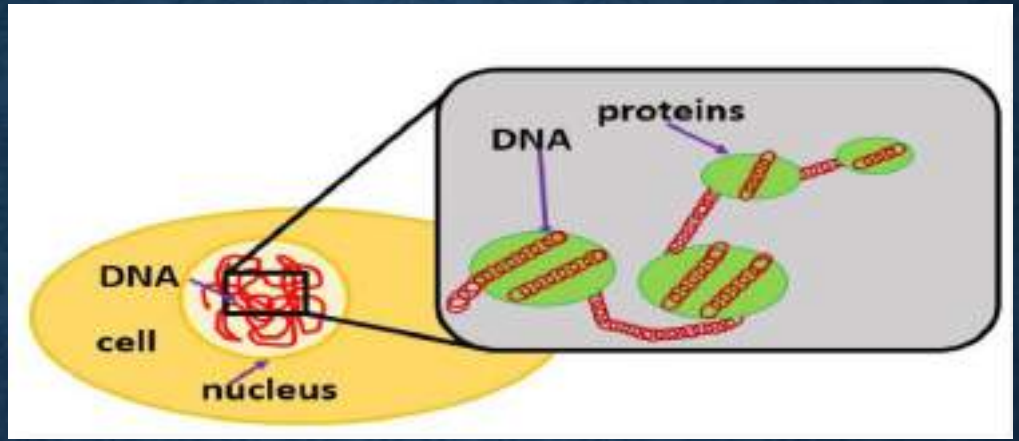

- **Isolation of DNA from Cells and Tissues**
- DNA can be extracted from many types of cells. The first step is to lyse or break open the cell. This can be done by grinding a piece of tissue in a blender. After the cells have broken open, a salt solution such as NaCl and a detergent solution containing the compound SDS (sodiumdodecyl sulfate) is added.

- **Isolation of Mitochondria from Cells and Tissues**
- Mitochondrial isolation protocols involve two processes – cell disruption to break open the cells and release the cellular structures, and differential centrifugation to recover fractions that are enriched for mitochondria

IN RAMAN IMAGING WE DO NOT NEED TO DISRUPT CELLS TO BREAK OPEN THE CELLS AND RELEASE THE CELLULAR STRUCTURES TO LEARN ABOUT THEIR BIOCHEMICAL COMPOSITION

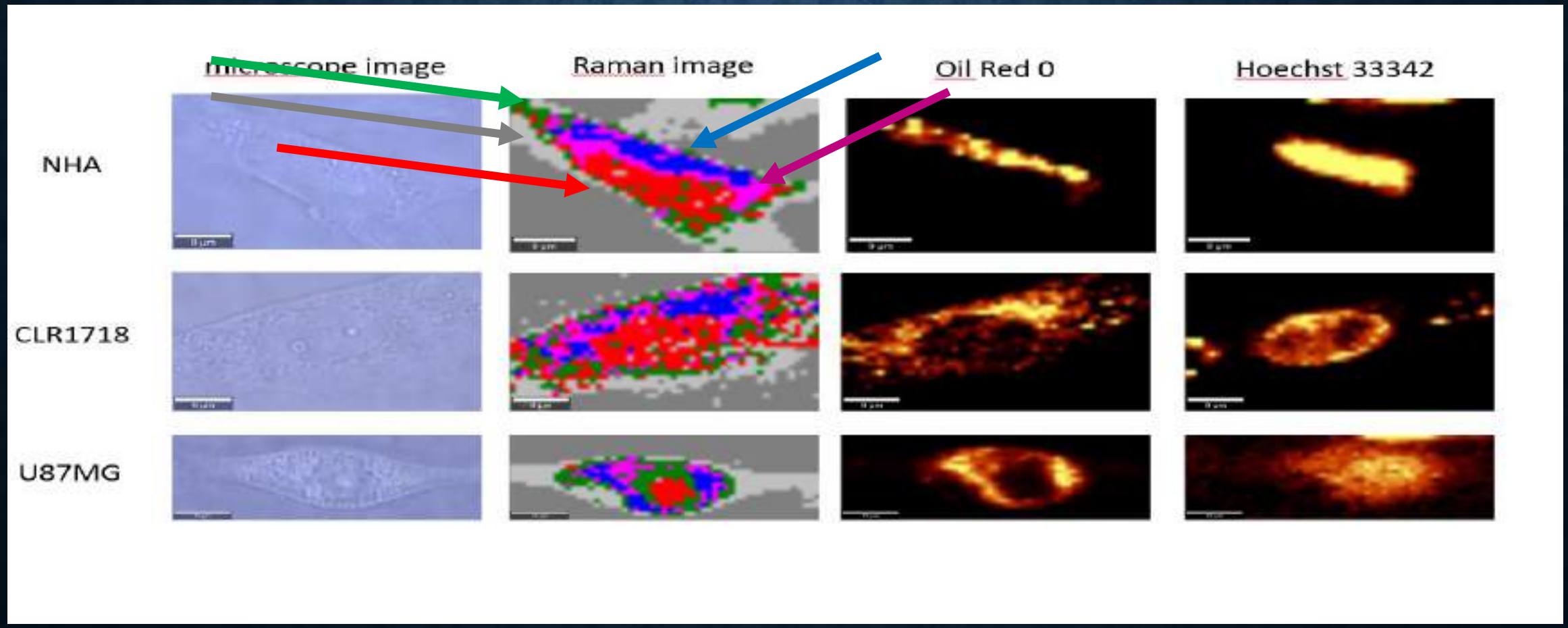

Abramczyk et al. LLSM, 2018

The real-time *in vivo* neurosurgical Raman system in our laboratory

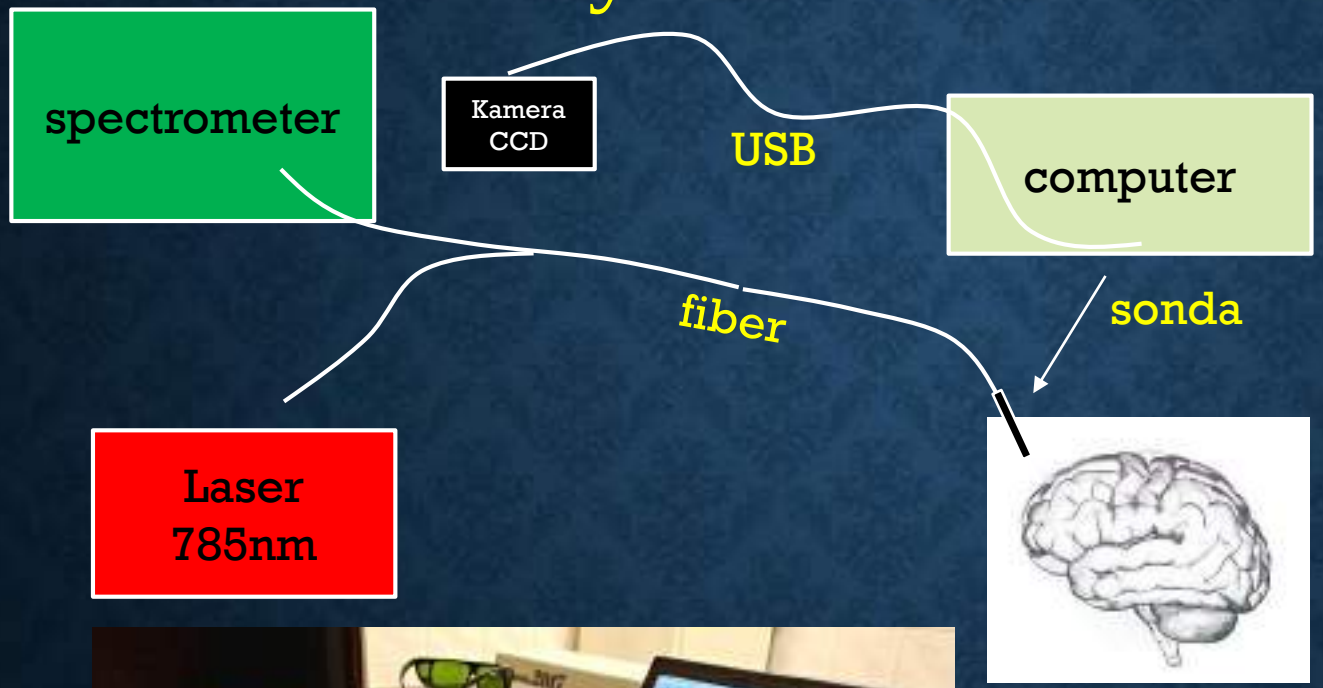

IN VIVO RAMAN OPTICAL BIOPSY ON RAT BRAIN IN LABORATORY OF LASER MOLECULAR SPECTROSCOPY

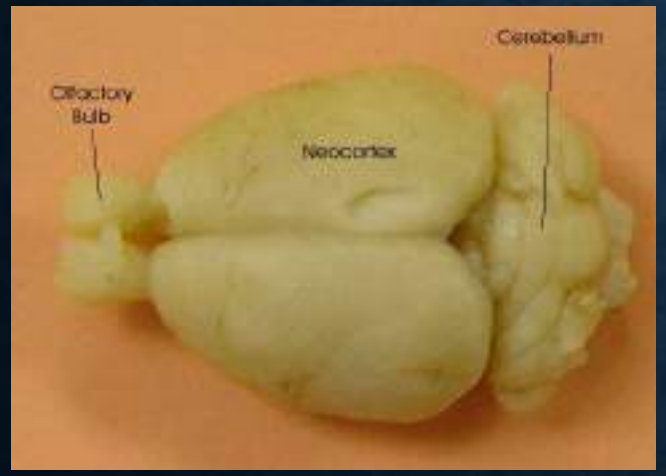

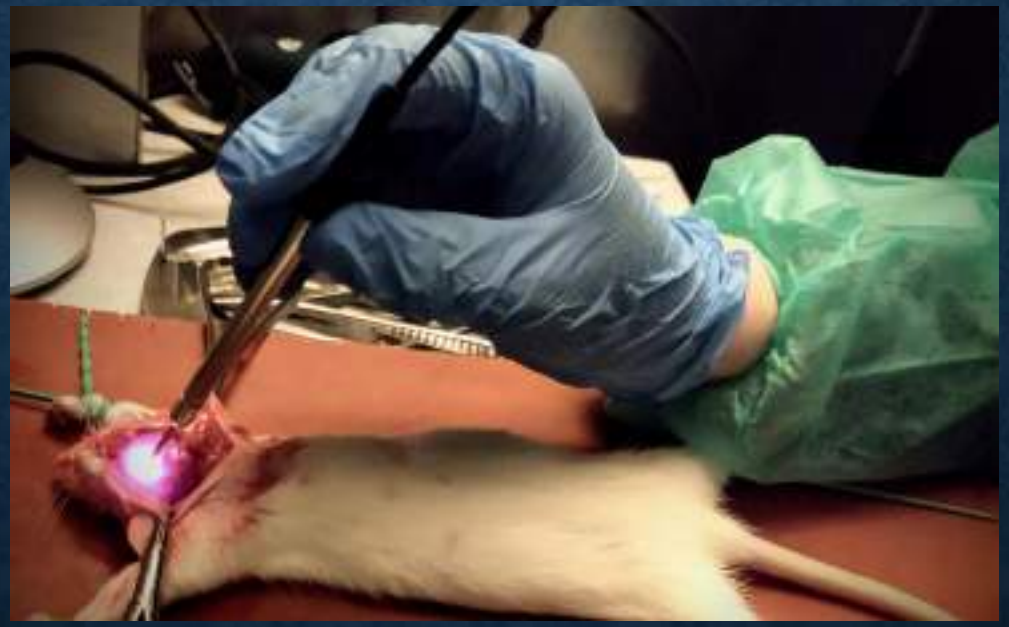

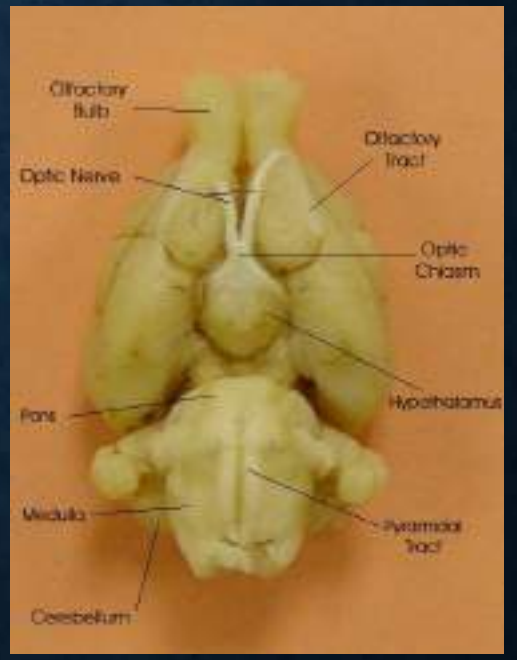

RAMAN SPECTROSCOPY GUIDES IN VIVO BRAIN OPTICAL BIOPSIES

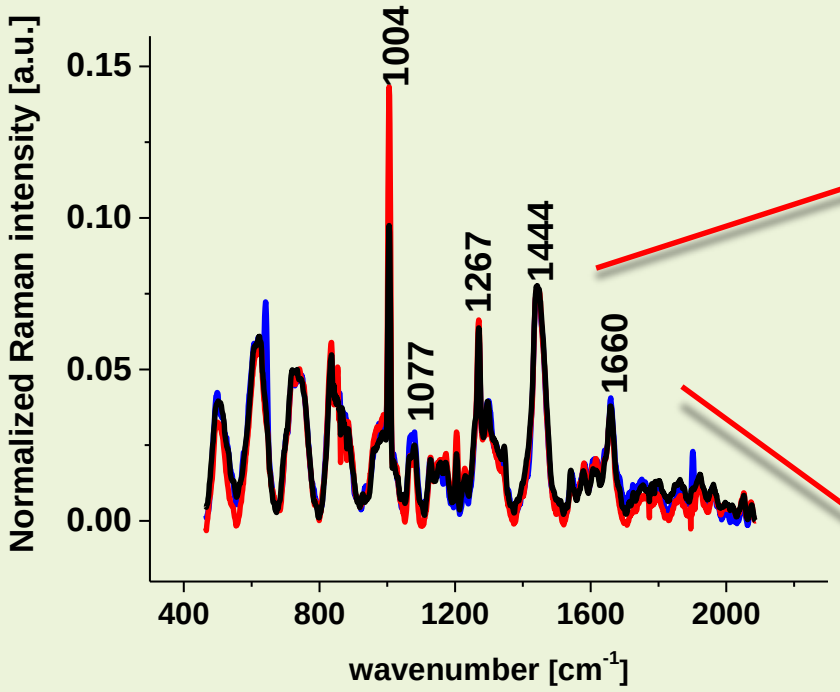

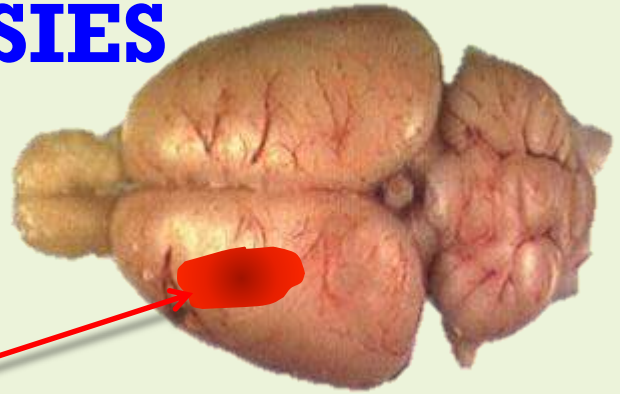

RAT BRAIN

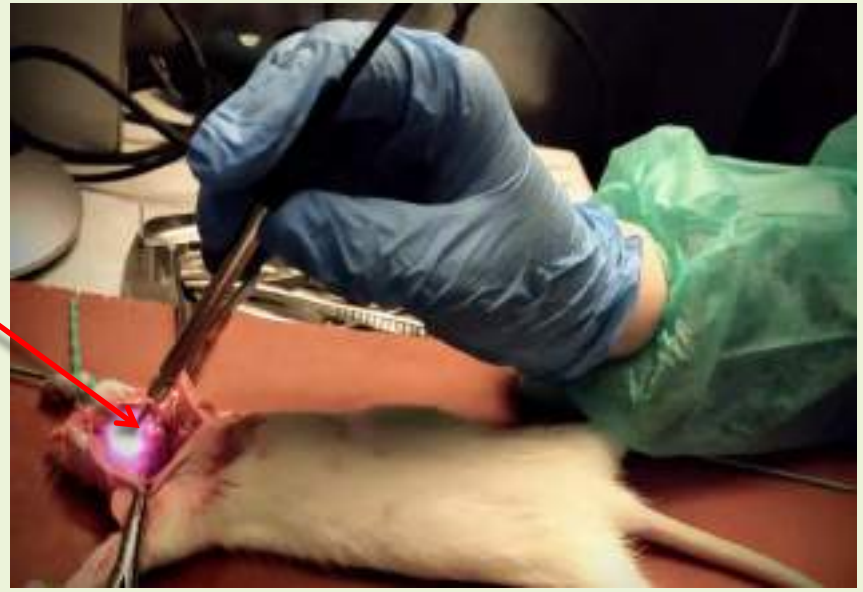

IN VIVO RAMAN OPTICAL BIOPSY IN RAT BRAIN IN LABORATORY OF LASER MOLECULAR SPECTROSCOPY

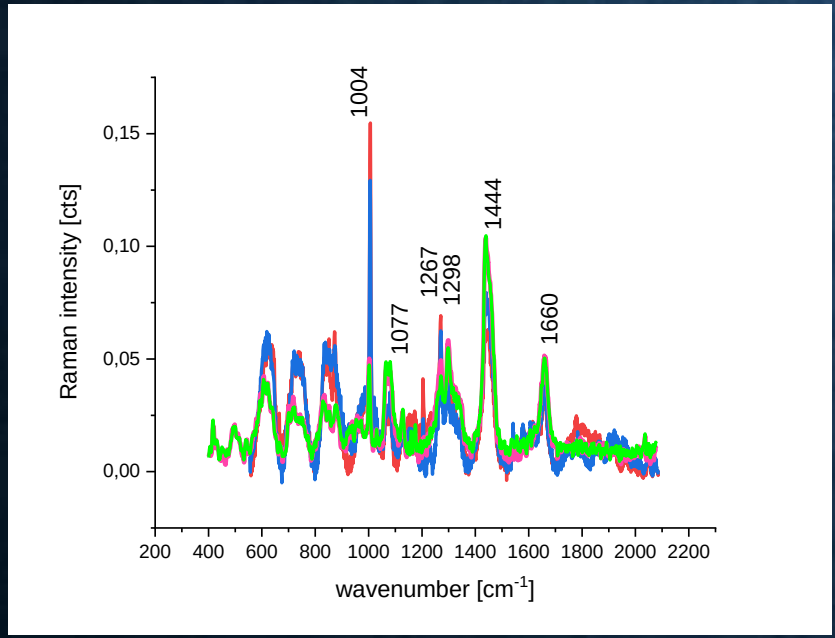

IN VIVO RAT BRAIN

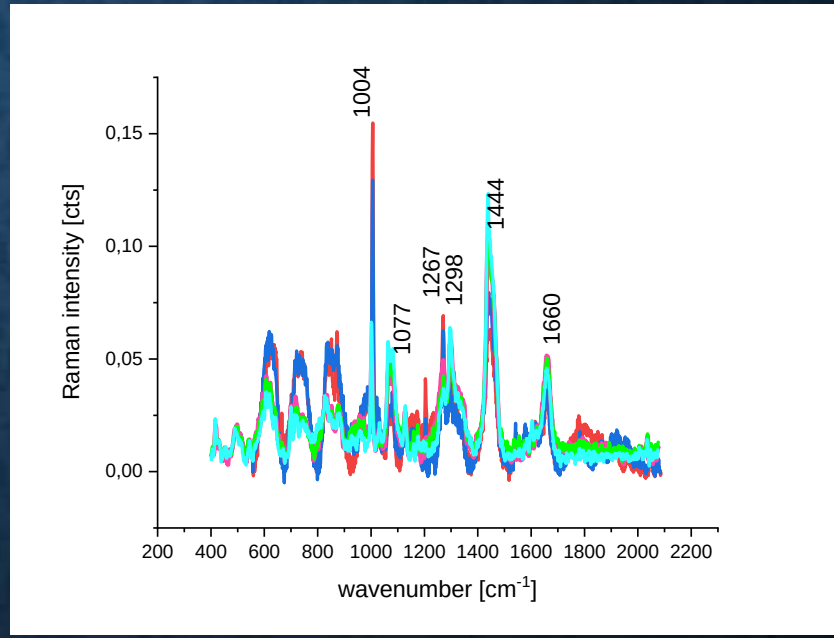

EX VIVO SWINE BRAIN

VISUALIZATION OF LIPISD DROPLETS CHEMISTRY

- While in some cases the morphology is a good indicator for metabolic changes in cells, it can be of equal importance to know cellular contents. In the case of LDs, changes in carbon saturation and chain length can be linked to diseases

TAG CHAIN LENGTH AND SATURATION MAPS IN SITU

- TAG saturation can be mapped in differentiated 3T3-L1 adipocytes from BCARS spectra using the ratio of 1650 cm-1 / 1450 cm-1 [232]. Di Napoli et al. show further that this ratio can be used both on phase-retrieved spectra and from raw CARS images along with 2930 cm-1 / 2885 cm-1 and 3010 cm-1 / 2855 cm-1 [233].

TAG CHAIN LENGTH AND SATURATION MAPS IN SITU

- The disadvantage of this ratio is that only one quantity for TAG chemistry, the number of double bonds, is determined while the chain length is not taken into consideration. In algae, it has been shown that the 1650 cm-1 / 1450
- cm- 1 from spontaneous Raman spectra can be correlated with number of double bonds and Nc=c/NCH2. This allows then the calculation of the chain length [235]. However, since the data is collected with spontaneous Raman spectroscopy, the measurements are slow causing low throughput.

TAG CHAIN LENGTH AND SATURATION MAPS IN SITU

- [232] H. A. Rinia, K. N. J. Burger, M. Bonn, and M. Müller, "Quantitative label-free imaging of lipid composition and packing of individual cellular lipid droplets using multiplex CARS microscopy.," Biophys. J., vol. 95, no. 10, pp. 4908–4914, 2008.
- [233] C. Di Napoli, I. Pope, F. Masia, P. Watson, W. Langbein, and P. Borri, "Hyperspectral and differential CARS microscopy for quantitative chemical imaging in human adipocytes," Biomed. Opt. Express, vol. 5, no. 5, pp. 1378–1390, 2014.
- [234] C. Di Napoli, I. Pope, F. Masia, W. Langbein, P. Watson, and P. Borri, "Quantitative Spatiotemporal Chemical Profiling of Individual Lipid Droplets by Hyperspectral CARS Microscopy in Living Human Adipose-Derived Stem Cells," Anal. Chem., vol. 88, no. 7, pp. 3677–3685, 2016.
- [235] H. Wu, J. V Volponi, A. E. Oliver, A. N. Parikh, B. A. Simmons, and S. Singh, "In vivo lipidomics using single-cell Raman spectroscopy.," Proc. Natl. Acad. Sci. U. S. A., vol. 108, no. 9, pp. 3809–14, 2011.
- [236] I. W. Schie, L. Nolte, T. L. Pedersen, Z. Smith, J. Wu, I. Yahiatène, J. W. Newman, and T. Huser, "Direct comparison of fatty acid ratios in single cellular lipid droplets as determined by comparative Raman spectroscopy and gas chromatography.," Analyst, vol. 138, no. 21, pp. 6662–6670, 2013. [

LIPID DROPLETS IN NORMAL MCF10A EPITHELIAL CELLS OF BREAST vs MILDLY MALIGNANT MCF7 AND AGRESSIVELY MALIGNANT MDA-MB-231

MCF10A - normal cells

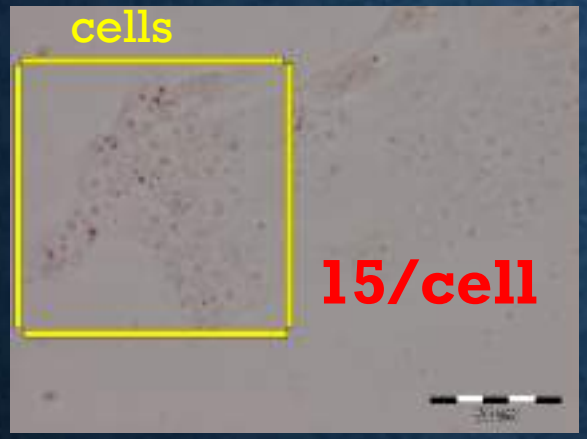

MCF7 - mildly malignant

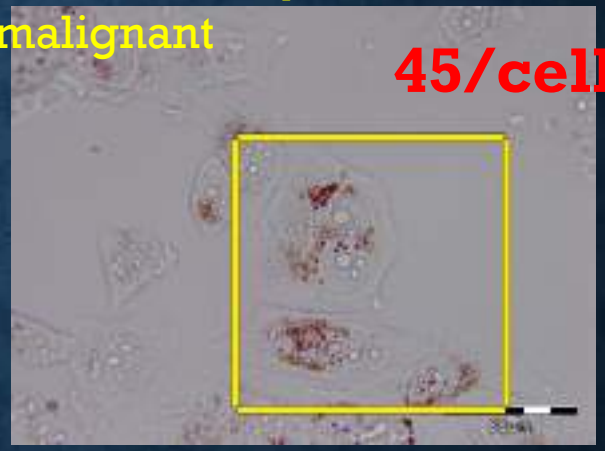

MDA-MB-231 - Agressively malignant

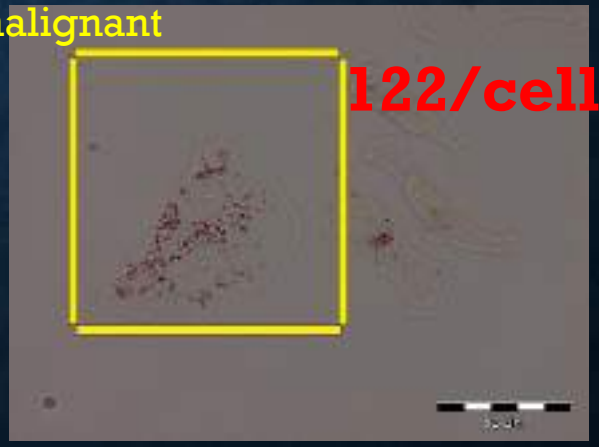

The goal of our study will be to assess the impact of cancer aggressiveness on the amount of cytosolic lipid droplets and their chemical composition in non-malignant and malignant human epithelial cell lines.

Abramczyk et al. Analyst, 2015

LIPID DROPLETS IN ASTROCYTES VS GLIOBLASTOMA U89

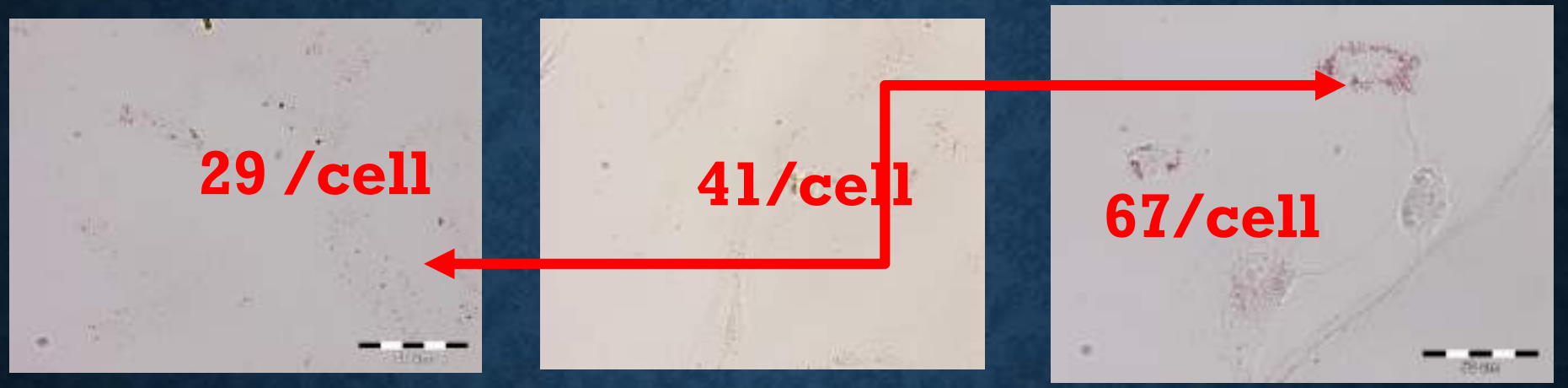

Astrocytes –normal cells

Astrocytoma –malignant cells

Glioblastoma U89- highly malignant cells

- Cancer cells contain increased numbers of lipid droplets compared with normal cells.
- Increased amount of lipid droplets correlates with increased aggressiveness of cancer.
- The increased amount of cytoplasmic lipid droplets in the human cancer cells may be closely related to increased rate of lipid synthesis in cancerous tissues.

Abramczyk et al. LLSM, 2018

THE SPATIAL DISTRIBUTION OF RETINOIDS IN NORMAL ASTROCYTES AND GLIOBLASTOMA CELLS

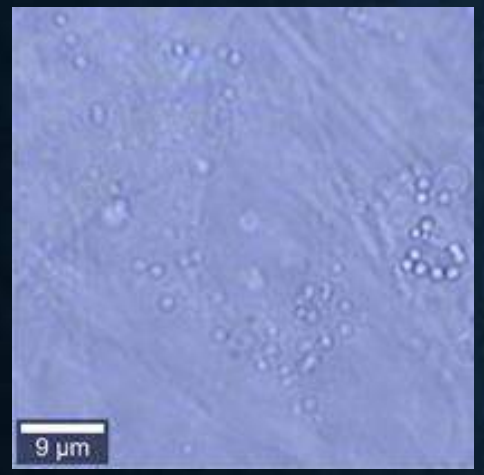

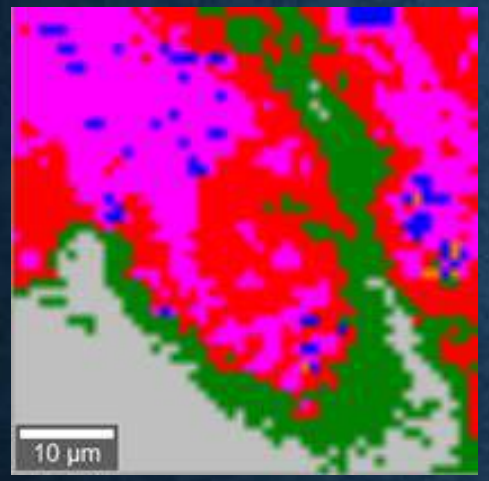

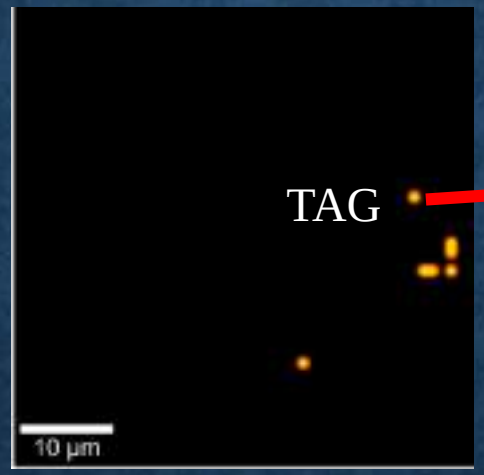

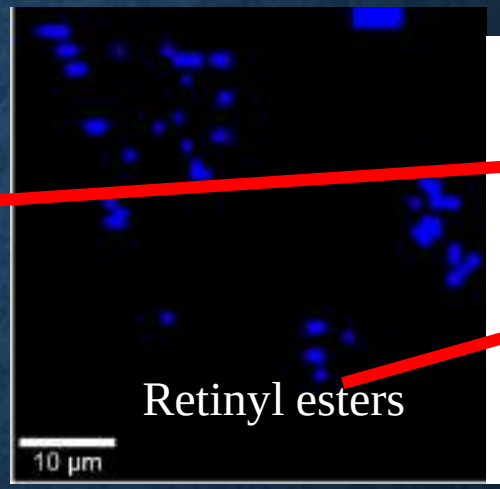

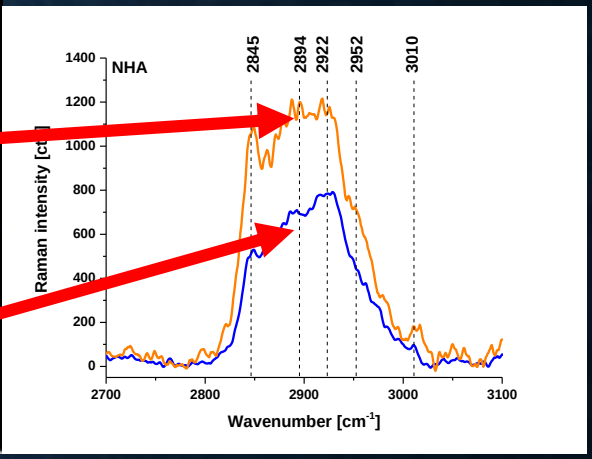

NORMAL ASTROCYTES

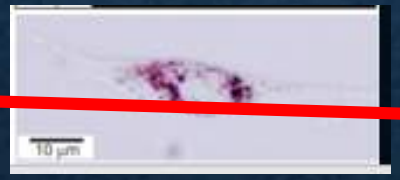

TAG

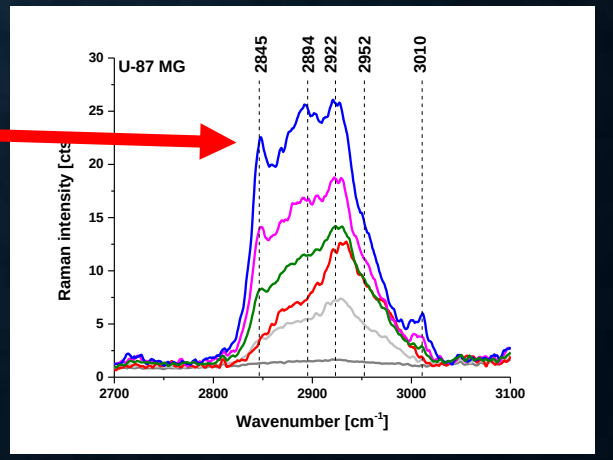

GLIOBLASTOMA

THE SPATIAL DISTRIBUTION OF RETINOIDS IN GLIOBLASTOMA CELLS: RETINOIDS IN MITOCHONDRIA, LIPID DROPLETS, NUCLEUS

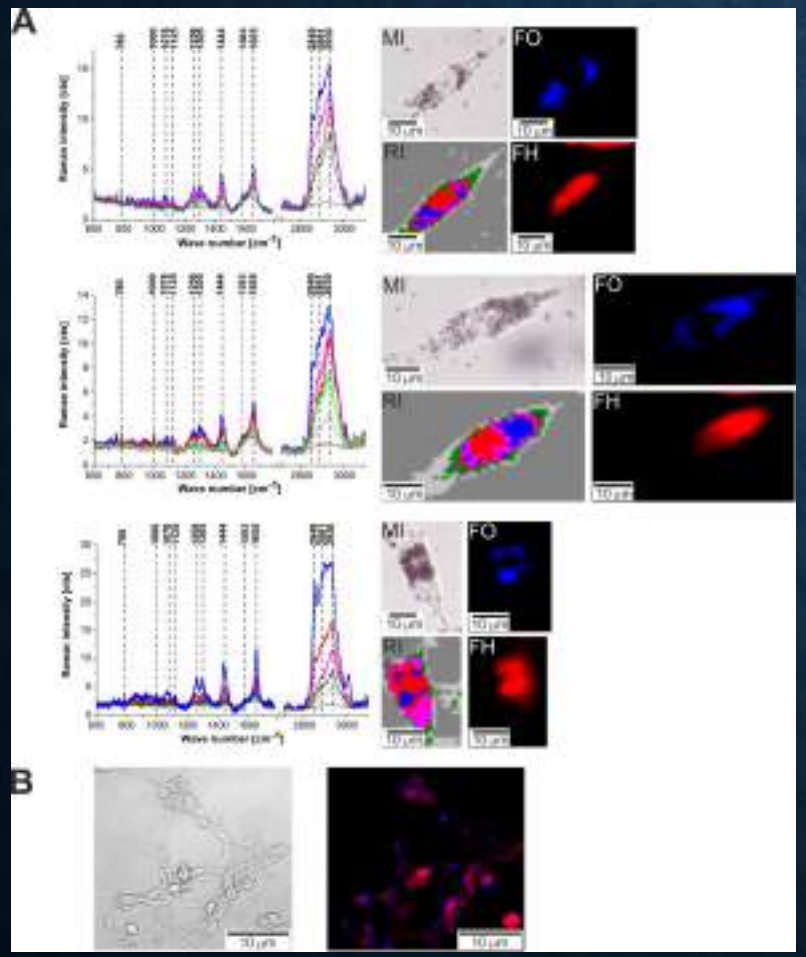

In Raman imaging we do not need to disrupt cells to break open the cells and release the cellular structures to learn about their biochemical composition in lipid droplets, nucleus, mitochondria

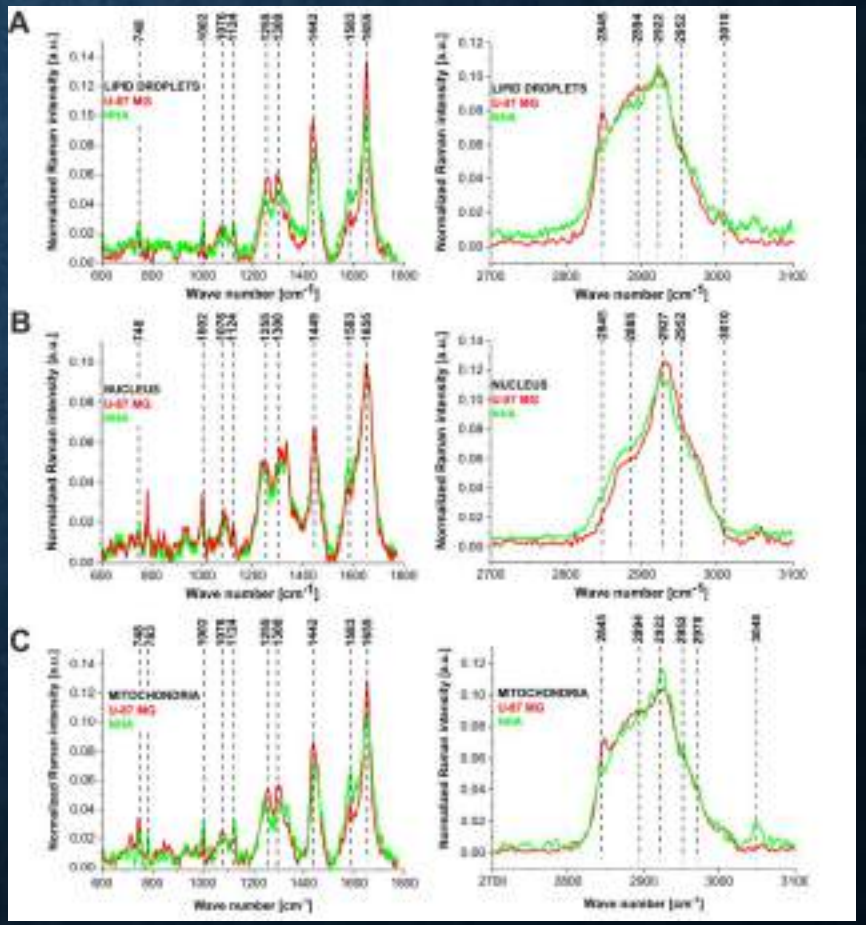

THE SPATIAL DISTRIBUTION OF RETINOIDS IN NORMAL ASTROCYTES AND GLIOBLASTOMA. RESONANCE RAMAN AND POLARIZATION SPECTRA

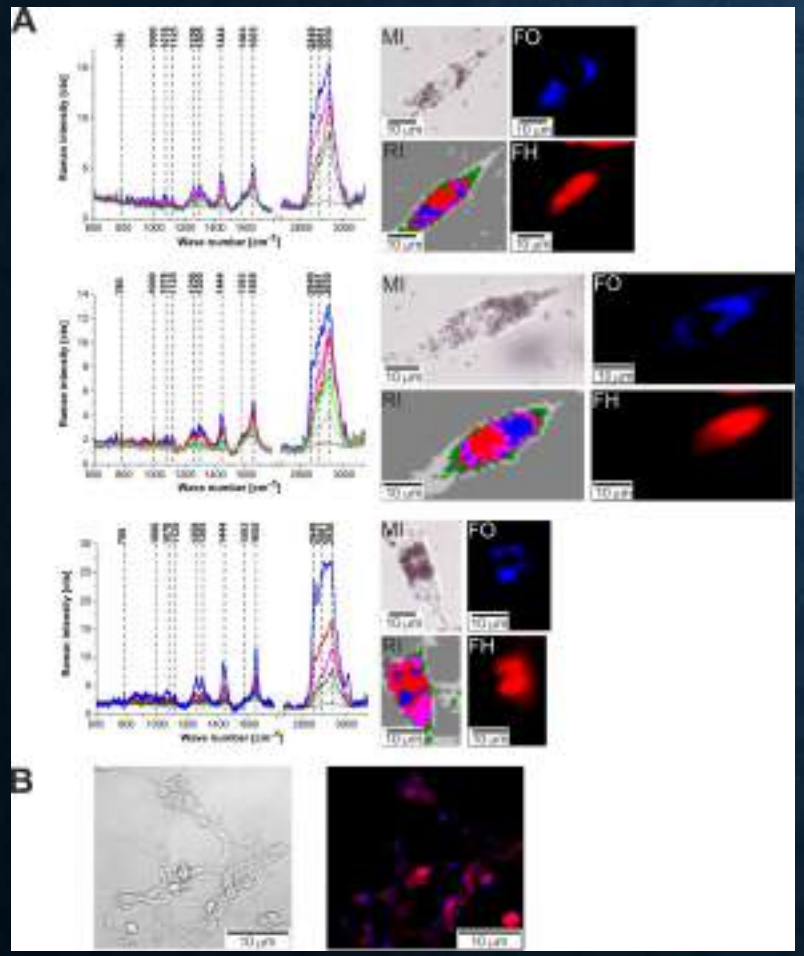

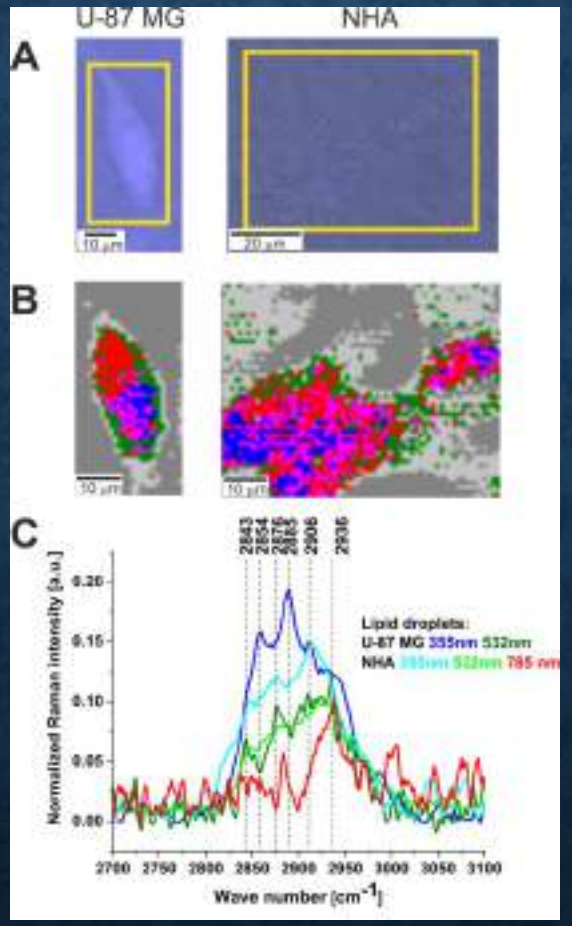

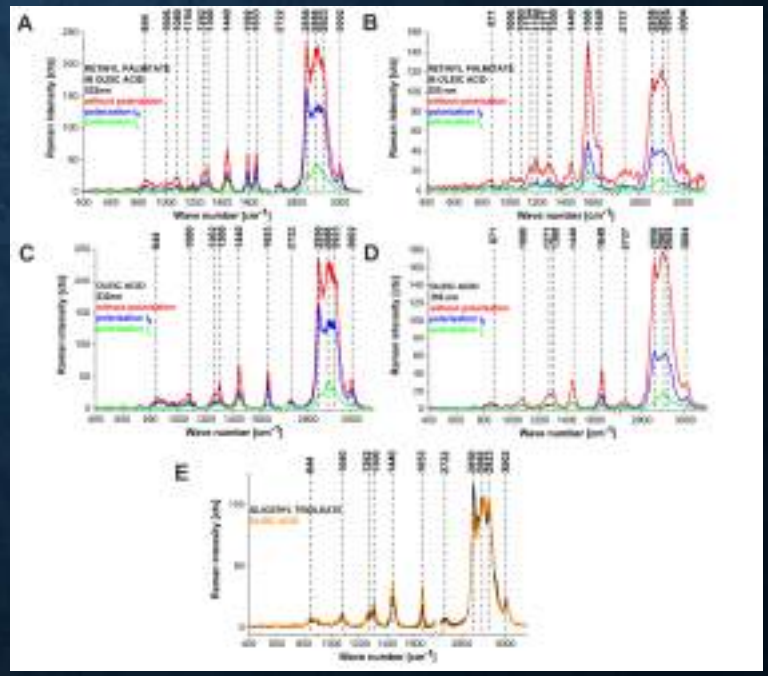

RAMAN IMIGINGTHE SPATIAL DISTRIBUTION OF RETINOIDS IN MEDULLOBLASTOMA (HUMAN BRAIN TISSUE) GRADE IV

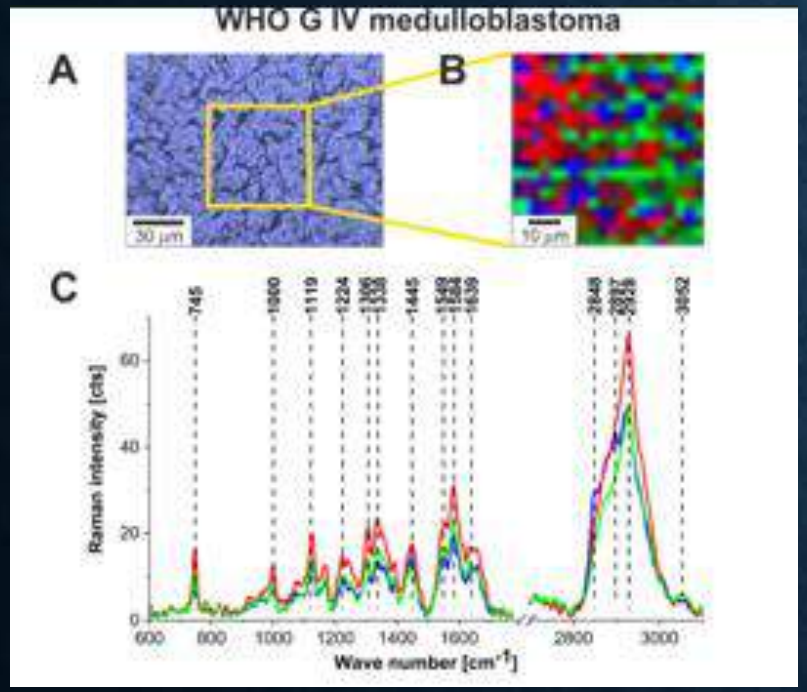

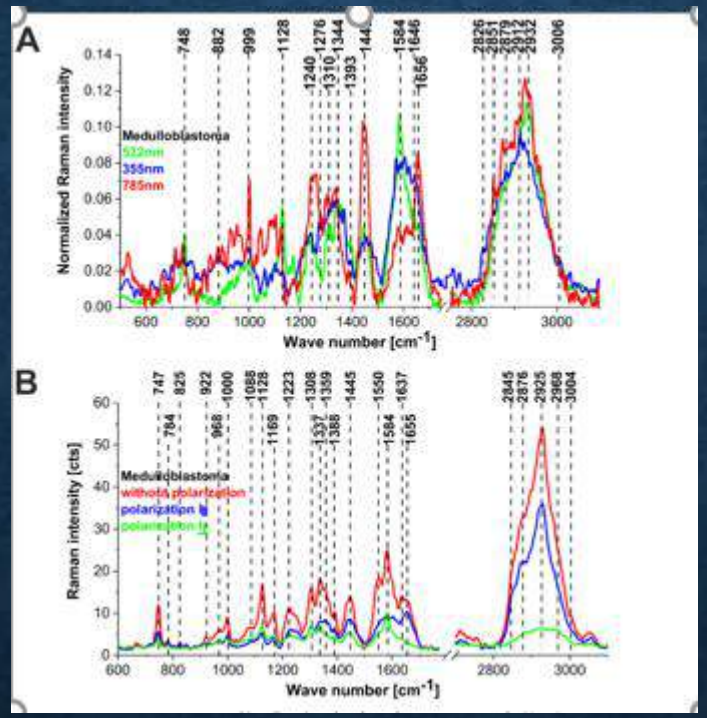

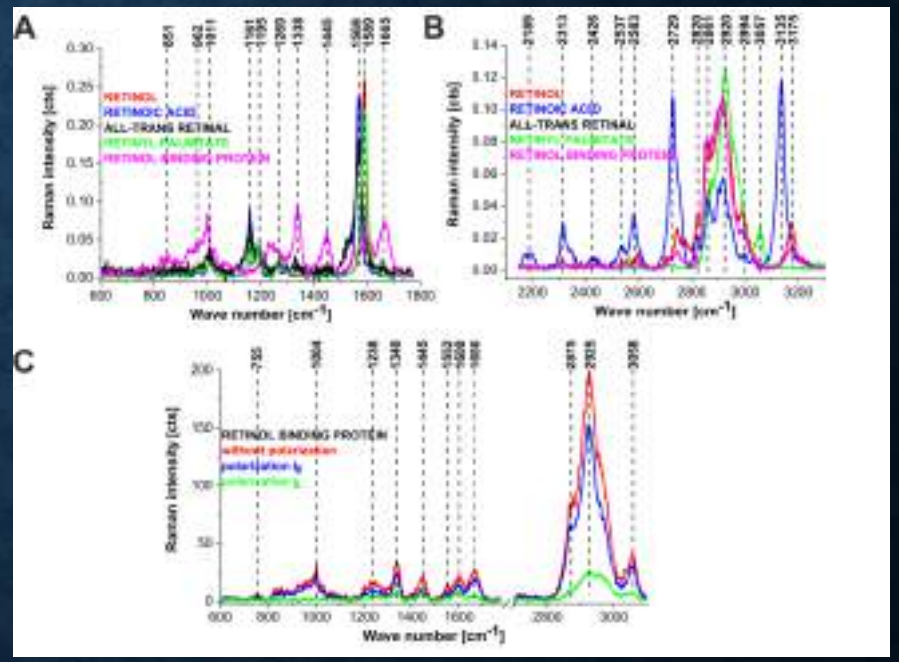

RAMAN AND MRI IMIGING THE SPATIAL DISTRIBUTION OF RETINOIDS IN ASTROCYTOMA (HUMAN BRAIN TISSUE) GRADE II/III

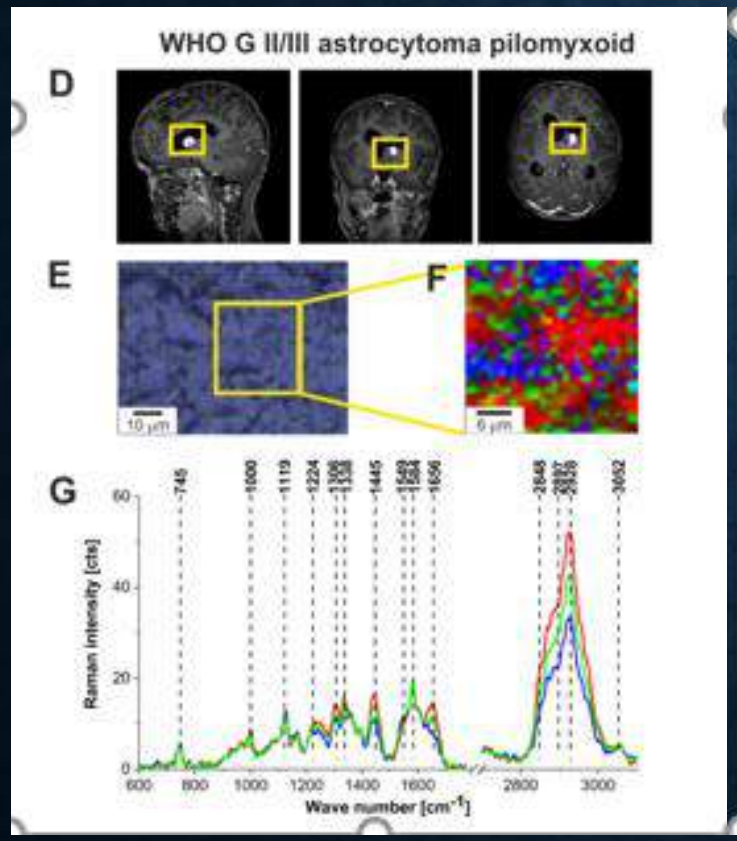

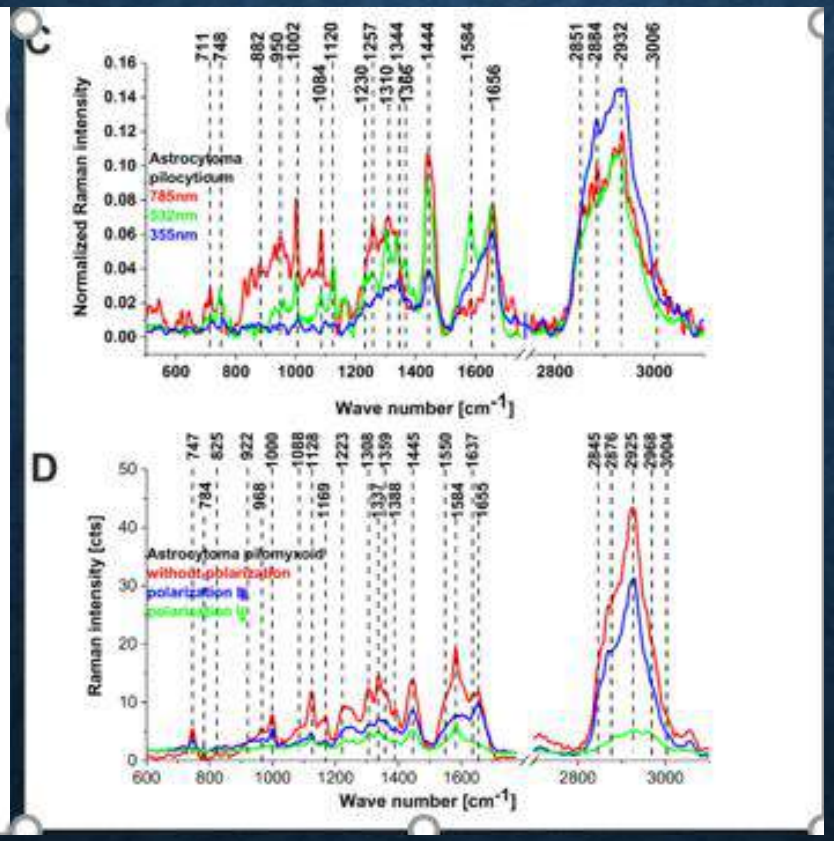

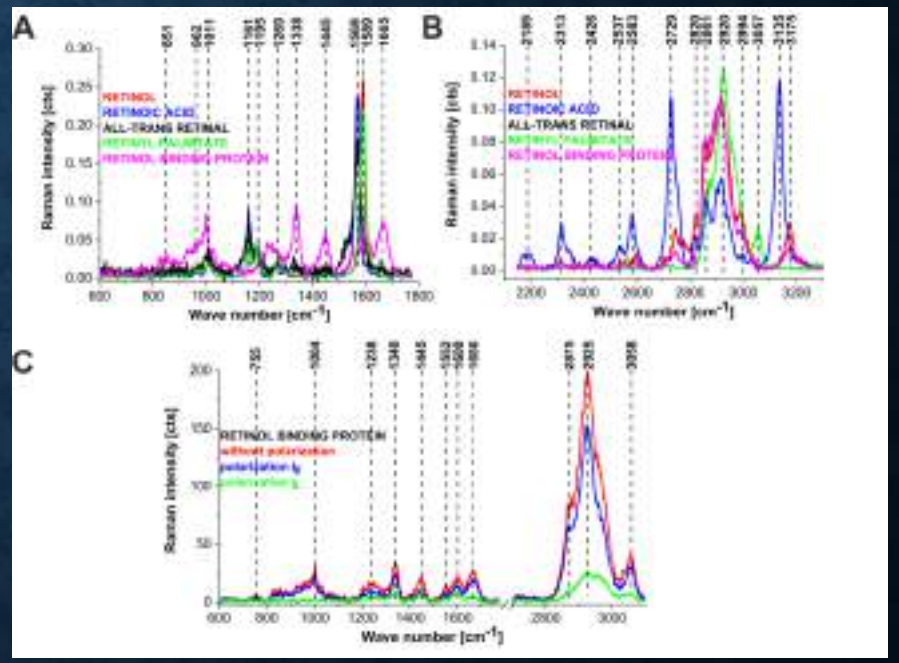

CONCLUSION

- Two types of lipid droplets in normal astrocytes and cancer cells of glioblastoma with distinct chemical compositions, biological functions and vibrational properties have been found.

- The two types of lipid droplets are related to different functions - energy storage and signalling. Their expression and biochemical composition depend on cancer aggressiveness.

- The first group is dominantly filled with TAGs and is involved in energy storage.
- The second group is mainly filled with retinyl esters and retinol binding proteins and is involved in signalling, especially JAK2/STAT6 pathway signalling.

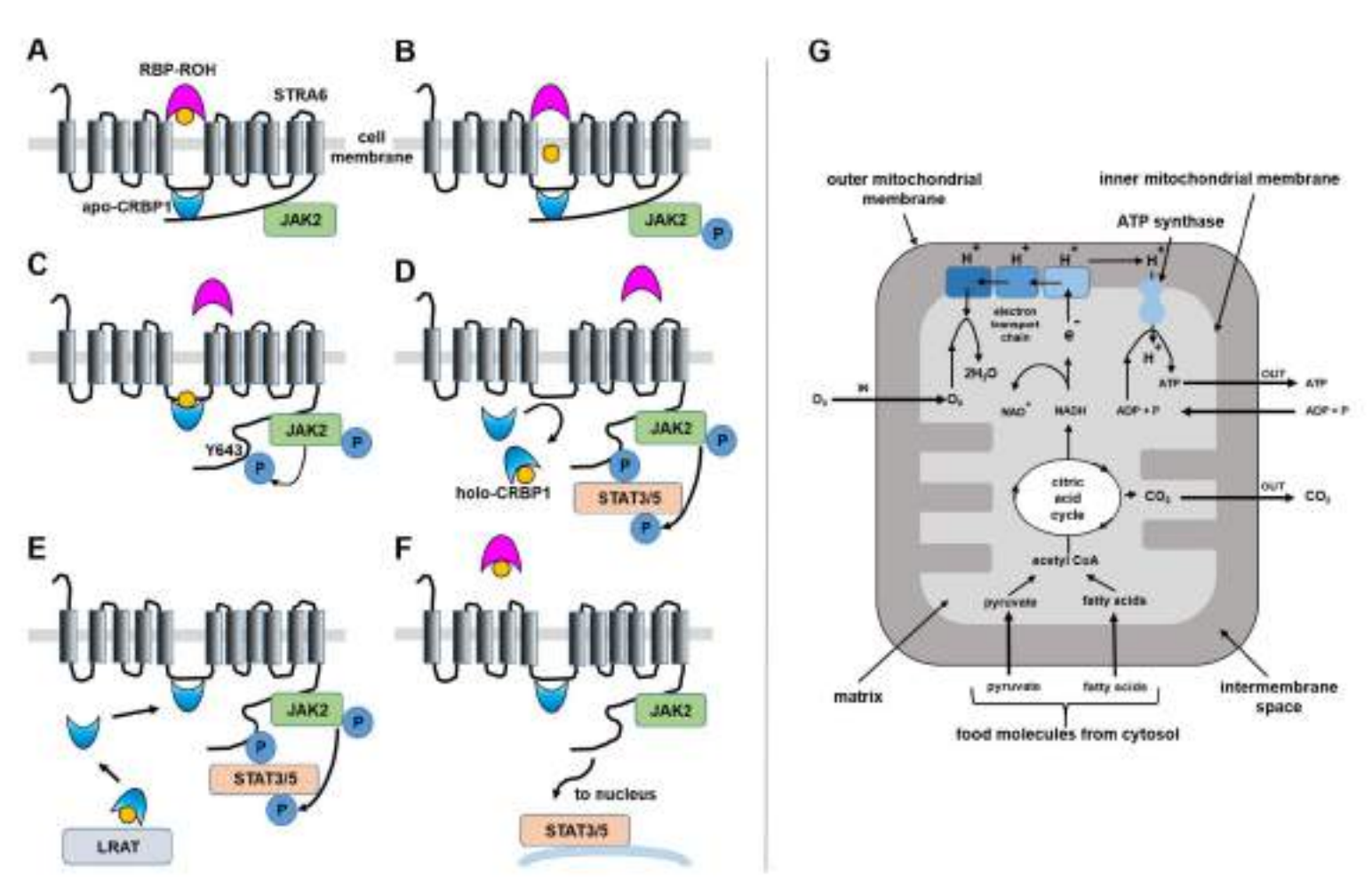

GENERAL CONCLUSION

Raman imaging, together with ultrafast time resolved spectroscopies are revealing functional aspects of retinoids at a new molecular level. These multidisciplinary approaches for free and protein bound retinoids combined with suitable cell cultures, ex vivo tissues, animal models can be especially helpful in translating these findings into therapeutic options for further development in animals and eventually in humans.

TIME RESOLVED SPECTROSCOPY AND STIMULATED RAMAN SPECTROSCOPY

stimulated Raman spectroscopy [158–161]. These methods should be able to help resolve the ongoing problems of understanding the pattern of carotenoid excited singlet states and their involvement in light harvesting. They should be able to resolve the key issues of which absorption changes reflect discrete electronic states and which come from different vibrational ones. Sorting this out will hopefully remove many of the current controversies.